OCEANOGRAPHY

Overturning circulation, nutrient limitation, and warming in the Glacial North Pacific

J. W. B. Rae[1]*, W. R. Gray[1,2], R. C. J. Wills[3], I. Eisenman[4], B. Fitzhugh[5], M. Fotheringham[1], E. F. M. Littley[1], P. A. Rafter[6], R. Rees-Owen[1], A. Ridgwell[7], B. Taylor[1], A. Burke[1]

Although the Pacific Ocean is a major reservoir of heat and CO_2, and thus an important component of the global climate system, its circulation under different climatic conditions is poorly understood. Here, we present evidence that during the Last Glacial Maximum (LGM), the North Pacific was better ventilated at intermediate depths and had surface waters with lower nutrients, higher salinity, and warmer temperatures compared to today. Modeling shows that this pattern is well explained by enhanced Pacific meridional overturning circulation (PMOC), which brings warm, salty, and nutrient-poor subtropical waters to high latitudes. Enhanced PMOC at the LGM would have lowered atmospheric CO_2—in part through synergy with the Southern Ocean—and supported an equable regional climate, which may have aided human habitability in Beringia, and migration from Asia to North America.

INTRODUCTION

Ocean circulation exerts a fundamental control on heat transport, marine biological productivity, and ocean-atmosphere CO_2 exchange (*1*). Today, the North Atlantic and North Pacific have contrasting circulation regimes, with vigorous deep-water formation in the North Atlantic, but only limited local ventilation in the North Pacific (*2*–*4*). This drives distinct patterns of CO_2 exchange, nutrient supply, and heat transport in each basin (*5*) and represents a first-order asymmetry in global biogeochemistry and climate (Fig. 1). It has been proposed that the circulation of the North Pacific was markedly different in past cold climates, but no consensus on this change exists. Proxies for ocean ventilation suggest enhanced intermediate water formation under glacial conditions (*6*–*11*) and local deep-water formation during Heinrich Stadial 1 (*12*, *13*). However, paired nutrient utilization and productivity proxies indicate reduced nutrient supply to the surface during cold climates (*14*, *15*), interpreted as the result of more stratified conditions with reduced ventilation. As the Pacific contains around half of the water in the global ocean and 30 times more carbon than the atmosphere, the lack of consensus on its behavior in different climate states represents a major gap in our understanding of the global climate system. Understanding the glacial climate of this region is also of interest for understanding the conditions under which early humans first migrated from Asia to North America around the end of the last ice age (*16*). Here, we use a compilation of sediment core proxy data for ocean ventilation, biological productivity, temperature, and salinity (see the Supplementary Materials for details), paired with Earth system modeling experiments, to shed new light on the circulation of the glacial North Pacific and its regional and global impact.

RESULTS AND DISCUSSION

Data compilation

To examine past changes in ventilation, we use proxies including $\delta^{13}C$ in benthic foraminifera (*6*, *17*), ^{14}C offsets between benthic

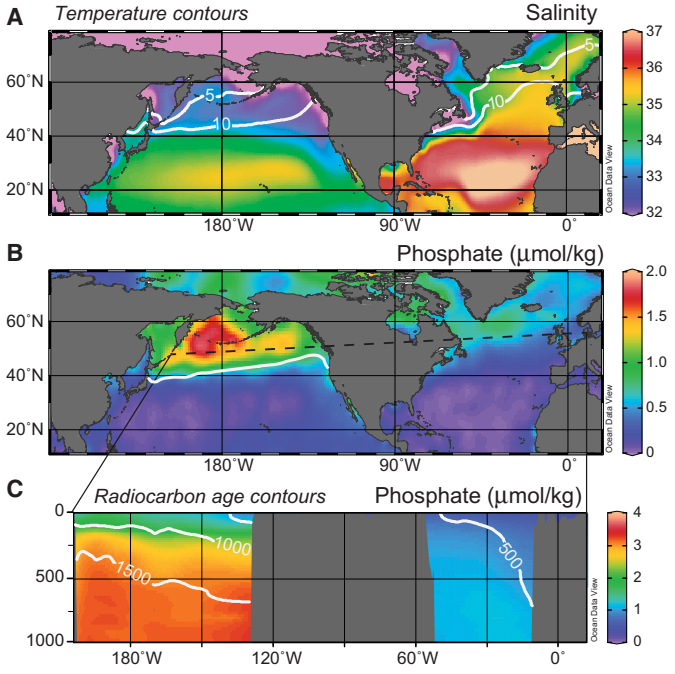

Fig. 1. Modern hydrography and nutrient content of the northern Pacific and Atlantic Oceans. (**A**) Sea surface salinity, with sea surface temperature contours for 5° and 10 °C. (**B**) Surface phosphate concentration, with a sea surface height contour to denote the subpolar gyre boundary. (**C**) Subsurface phosphate concentration along a zonal section indicated by the dashed line in (B), with pre-bomb radiocarbon age contours. Note the relative isolation of the subpolar gyre in the North Pacific, which allows pooling of cold, fresh water in the surface, and old, nutrient-rich waters to upwell from below. In contrast, the active overturning circulation of the North Atlantic flushes warm, salty, nutrient-poor water from the subtropics through the upper reaches of this well-ventilated basin. Salinity, temperature, and phosphate data are gridded annual averages from WOA09; radiocarbon data from Global Ocean Data Analysis Project version 2 [GLODAPv2 (*101*)]; and sea surface height from (*159*).

[1]School of Earth and Environmental Sciences, University of St Andrews, St Andrews, UK. [2]Laboratoire des Sciences du Climat et de l'Environnement (LSCE/IPSL), Université Paris-Saclay, Gif-sur-Yvette, France. [3]Department of Atmospheric Sciences, University of Washington, Seattle, WA 98195, USA. [4]Scripps Institution of Oceanography, University of California, San Diego, La Jolla, CA 92093, USA. [5]Department of Anthropology, University of Washington, Seattle, WA 98195, USA. [6]Department of Earth System Science, University of California, Irvine, Irvine, CA 92697, USA. [7]Department of Earth Sciences, University of California, Riverside, Riverside, CA 92521, USA. *Corresponding author. Email: jwbr@st-andrews.ac.uk

and planktic foraminifera (*18*, *19*), and various redox tracers (*7*). These data indicate that waters below ~2000 m are poorly ventilated at the Last Glacial Maximum (LGM), with lower $\delta^{13}C$, ^{14}C, and oxygen (Figs. 2A and 3). This is consistent with previous interpretations of the deep glacial Pacific as a likely store of glacial CO_2 (*1*, *20*). In contrast, waters above ~2000 m show enhanced ventilation (Figs. 2A and 3). This is seen across all tracers, with 73% of the 72 sites above 2000 m indicating increased ventilation, 17% showing no change outside of 1σ uncertainty, and only 10% indicating reduced ventilation. This suggests a substantial increase in North Pacific Intermediate Water (NPIW) formation at the LGM (*6*). This result is further supported by profiles of $\delta^{18}O$ in benthic foraminifera (*6*, *11*): In contrast to the modern, where a smooth and modest increase in $\delta^{18}O$ with depth suggests a dominantly diffusive regime, LGM profiles (*6*, *11*) exhibit a notable transition at ~2000-m water depth (Fig. 3A). This indicates a sharp transition in temperature and/or $\delta^{18}O_{sw}$, which, as conservative tracers, provide evidence of a physical water mass boundary (*21*), with increased advection of NPIW overcoming the smoothing influence of diffusion. A local source of intermediate waters in the glacial North Pacific is also supported by meridional sections of benthic ^{14}C age and $\delta^{13}C$ (Fig. 3 and fig. S3), which show the spread of well-ventilated waters from the surface into the ocean's interior.

To examine changes in sea surface temperatures (SSTs), we use Mg/Ca in planktic foraminifera and the alkenone saturation index $U^{K'}_{37}$. SSTs in the subtropical gyre are cooler at the LGM, as expected for glacial conditions, and there is a large midlatitude cooling due to the southward expansion of the subpolar gyre (Fig. 2C and fig. S4) (*22*). In contrast, LGM temperatures in the subpolar gyre are either similar to or warmer than today (80% of records show warmer temperatures or no significant change), with ~2°C warming observed in the western North Pacific (Fig. 2C and figs. S1C and S4) (*23*, *24*). These warm SSTs require a circulation change to counter lower CO_2 and greater ice coverage (*25*) at the LGM and are consistent with enhanced heat transport by an invigorated Pacific Meridional Overturning Circulation (PMOC).

Sea surface salinity change at the LGM is estimated using $\delta^{18}O$ in planktic foraminifera, corrected for temperature using Mg/Ca and for whole-ocean $\delta^{18}O$/salinity change. Increased salinity is indicated throughout the North Pacific subpolar gyre (Fig. 2D and fig. S4), which would have aided intermediate water formation.

To reconstruct changes in export productivity, we use sedimentary opal and biogenic barium contents (*26*). All data poleward of 40°N indicate a reduction in glacial export productivity (Fig. 2B and fig. S1B). However, tracers of nutrient utilization (e.g., $\delta^{15}N$) suggest that biological nutrient drawdown was more complete (*15*). For more complete nutrient drawdown to be achieved despite reduced export productivity, the pool of available major nutrients (phosphate, nitrate, and silicic acid) must have been smaller (*1*, *15*). This is further supported by considering that micronutrient (e.g., iron) availability, which partially limits productivity in the North Pacific today,

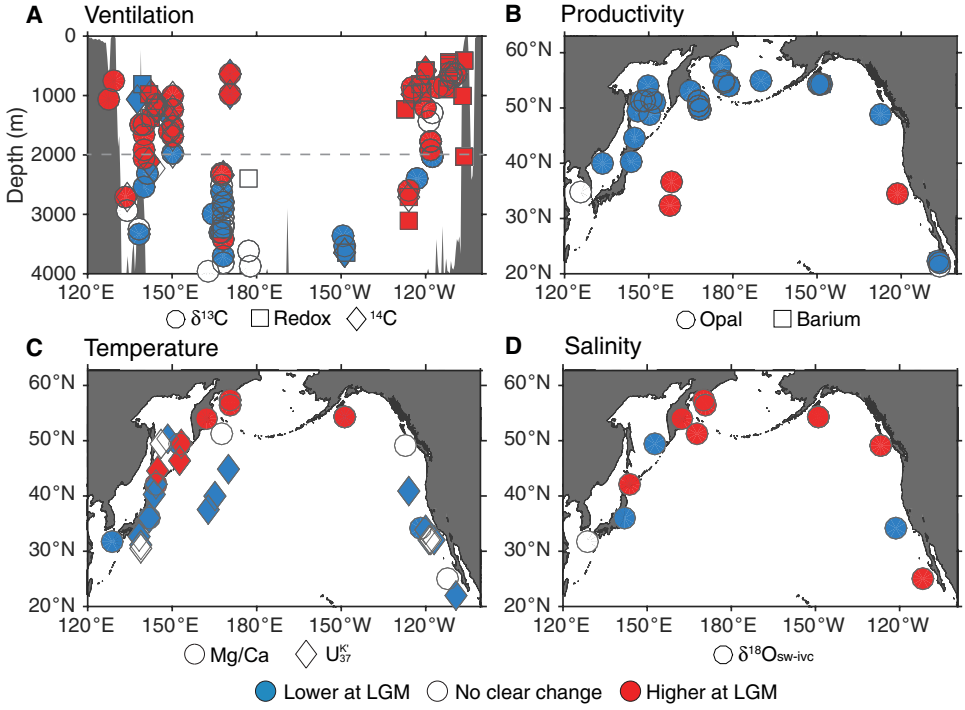

Fig. 2. Reconstructions of changes in ventilation, export productivity, temperature, and salinity at the LGM relative to the Holocene. Red indicates an increase at the LGM relative to the Holocene, blue a decrease, and white no clear change outside of 1σ uncertainty (see the Supplementary Materials for details of data compilation). (**A**) Ventilation proxies, including $\delta^{13}C$ (circles), radiocarbon (diamonds), and a variety of redox tracers (squares), taken from sites above 20°N. (**B**) Export productivity proxies, including sediment core opal (circles) and biogenic barium (squares) contents. (**C**) Sea surface temperature proxies, including planktic foraminiferal Mg/Ca (circles) and alkenone saturation index UK'37 (diamonds). (**D**) Change in sea surface salinity, derived from paired $\delta^{18}O$ and Mg/Ca data on planktic foraminifera, corrected for whole-ocean $\delta^{18}O$ and salinity changes due to ice volume. At the LGM, North Pacific intermediate waters are better ventilated, and productivity in the subpolar North Pacific is lower. An increase in salinity is seen throughout the North Pacific, and although the subtropical gyre cools, the subpolar North Pacific shows an anomalous warming, despite peak glacial conditions. See fig. S1 for an alternative presentation of these data.

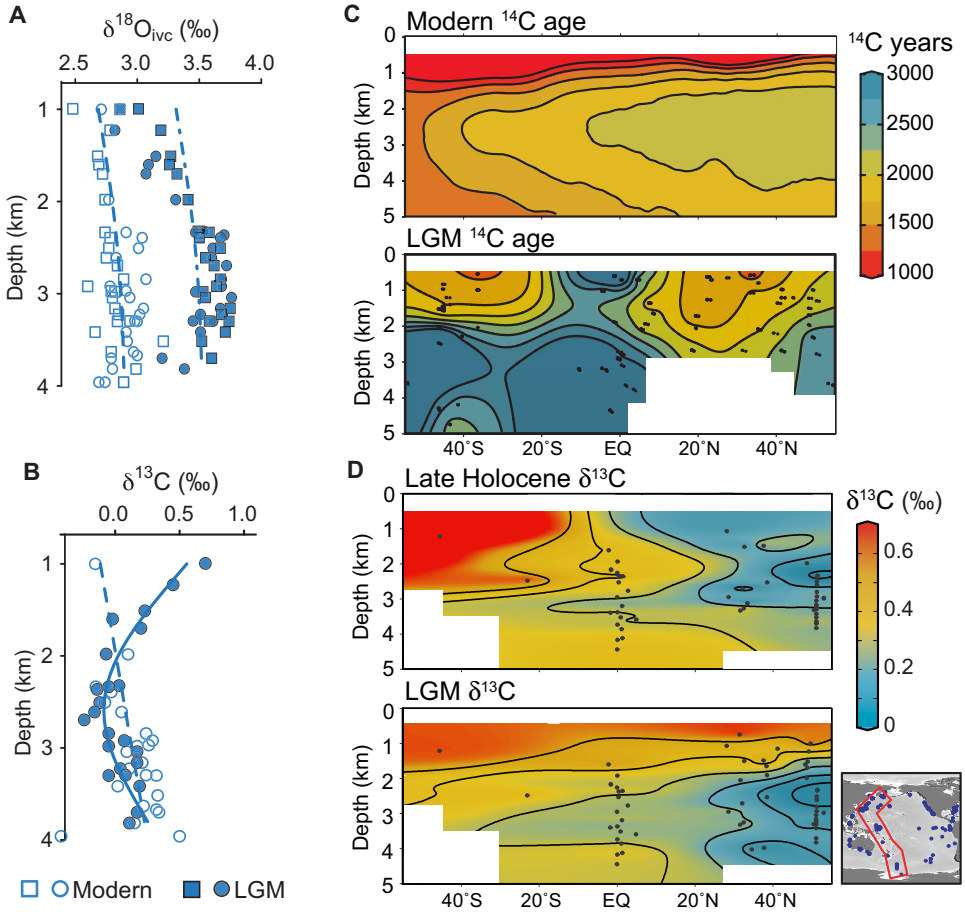

Fig. 3. Profiles and meridional sections of proxies for deep ocean circulation. The $\delta^{18}O$ profile (**A**) uses *Cibicidoides* spp. (circles) and *Uvigerina* spp. (squares), with *Uvigerina* data corrected for vital effects by –0.47‰ (*160*); the $\delta^{13}C$ profile (**B**) uses *Cibicidoides* spp. only; profile data are from the NW Pacific (*6*). LGM $\delta^{13}C$ data (in B and D) and $\delta^{18}O$ are corrected for the –0.34 and 1‰ whole ocean changes in $\delta^{13}C$ and $\delta^{18}O_{sw}$ (*17*). Generalized additive model fits are shown for Holocene $\delta^{13}C$ and $\delta^{18}O$ (dashed lines) and LGM $\delta^{13}C$ (solid line) (*161*). The thin dotted-dashed line through the LGM $\delta^{18}O$ data in (A) is the Holocene $\delta^{18}O$ fit with a +0.6 ‰ offset; while the Holocene $\delta^{18}O$ profile increases smoothly with depth, the LGM data exhibit a marked transition at ~2000 m, indicative of a water mass boundary. ^{14}C data in (**C**) are shown as ^{14}C age relative to the contemporaneous atmosphere, with modern data from GLODAPv2 and LGM data from benthic foraminifera (see Materials and Methods for details). $\delta^{13}C$ section data in (**D**) are from the western Pacific (*17*)—see inset map. Locations of sediment core data are shown in black dots and areas of poor data coverage in white, and further details are given in figs. S2 and S3.

was enhanced because of higher dust fluxes (*27*). The decrease in export productivity in the LGM North Pacific thus requires a decrease in major nutrient supply.

Mechanisms for glacial nutrient limitation

Previous studies have suggested that nutrient limitation in the glacial North Pacific was driven by enhanced freshwater stratification in surface waters under a colder climate (*14*, *15*). However, this suggestion is difficult to reconcile with our evidence for enhanced intermediate water formation (Figs. 2A and 3) and saltier, warmer surface waters (Fig. 2, C and D, and fig. S4). An alternative model is thus required for large-scale changes in nutrients and circulation in the northern subpolar basins.

To explore controls on circulation and nutrient supply in the North Pacific, we first consider modern phosphate concentrations in an adaptation of Warren's box model [(*2*, *3*); the Supplementary Materials], which was previously used to demonstrate that the low salinity that currently stratifies the subpolar North Pacific is a result of low evaporation rates relative to precipitation, as well as minimal exchange with the saltier subtropical gyre (*2*–*4*). Isolation of the subpolar gyre also contributes to high surface nutrients in the modern North Pacific, by limiting the input of low-nutrient water from the subtropics (fig. S5). Although salinity stratification limits the depth of convection, subsurface waters are still brought to the surface via wind and tidally driven mixing, wintertime convection, and Ekman suction (*5*). As these subsurface waters have been long isolated in the deep ocean, they are extremely rich in nutrients acquired through remineralization, with little input of low-nutrient subtropical water or newly ventilated intermediate water to dilute this potent subsurface nutrient reservoir (Fig. 1C). This contrasts with the North Atlantic, where a less zonal wind-stress pattern and an active overturning circulation supplies warm, salty, and nutrient-poor subtropical water to high latitudes (Fig. 1). Subduction of this water creates nutrient-poor intermediate and deep waters and effectively flushes nutrients from the upper reaches of the modern North Atlantic.

Thus, today we have two realizations of basin-scale nutrient dynamics and circulation at high northern latitudes: The Pacific is stratified and poorly ventilated, with cold, fresh, and nutrient-rich surface waters, supplied by upwelling of old, nutrient-rich waters from below, while the Atlantic is well ventilated, with a vigorous overturning circulation that flushes warm, salty, and nutrient-poor waters from the subtropics through its upper reaches. At the LGM, our data show that the North Pacific was better ventilated, had lower nutrients, and was saltier and warmer. This is consistent with a more Atlantic-like circulation regime, with enhanced overturning down to ~2000-m depth.

Modeling experiments

The ability of enhanced overturning to reduce nutrient supply to the surface of the glacial North Pacific is further supported by a series of experiments with an Earth system model (cGENIE) and tests with a simple box model (see the Supplementary Materials). We simulate Pacific overturning in cGENIE by reducing the prescribed transport of fresh water from the North Atlantic to the North Pacific. As the North Pacific gets saltier, its meridional overturning circulation increases (fig. S6), driving a decrease in surface and subsurface nutrients (Fig. 4 and figs. S5 and S7) due to increasing input of nutrient-poor subtropical waters. Although convective mixing increases and stratification is reduced (Fig. 4C), the dilution of the subsurface nutrient reservoir by freshly ventilated waters has a much larger effect (Fig. 4 and figs. S5 and S7; see Materials and Methods). This pattern is observed across different model base states and is also seen in the higher-resolution LOVECLIM and UVic Earth system models (fig. S8) (*28*). Recent work using the Paleoclimate Modelling Intercomparison Project (PMIP3) ensemble shows that Ekman suction in the glacial North Pacific was around 60% higher than today (*29*). Given this increase in upwelling, a substantial decrease in the nutrient content of the upwelled water is required to result in lower surface nutrient concentrations; our modeling results show this can be effectively achieved by enhanced overturning circulation.

Pacific overturning and biogeochemistry during other climate states

The presence or absence of a PMOC may help explain biogeochemical transitions in other time intervals. For example, the peak in nutrient supply during the Bølling-Allerød warm interval [14.7 to 12.9 thousand years ago (ka)] appears to be associated with an abrupt decrease in PMOC (*12*, *29*), while the decrease in export productivity and increase in SST during intensification of Northern Hemisphere

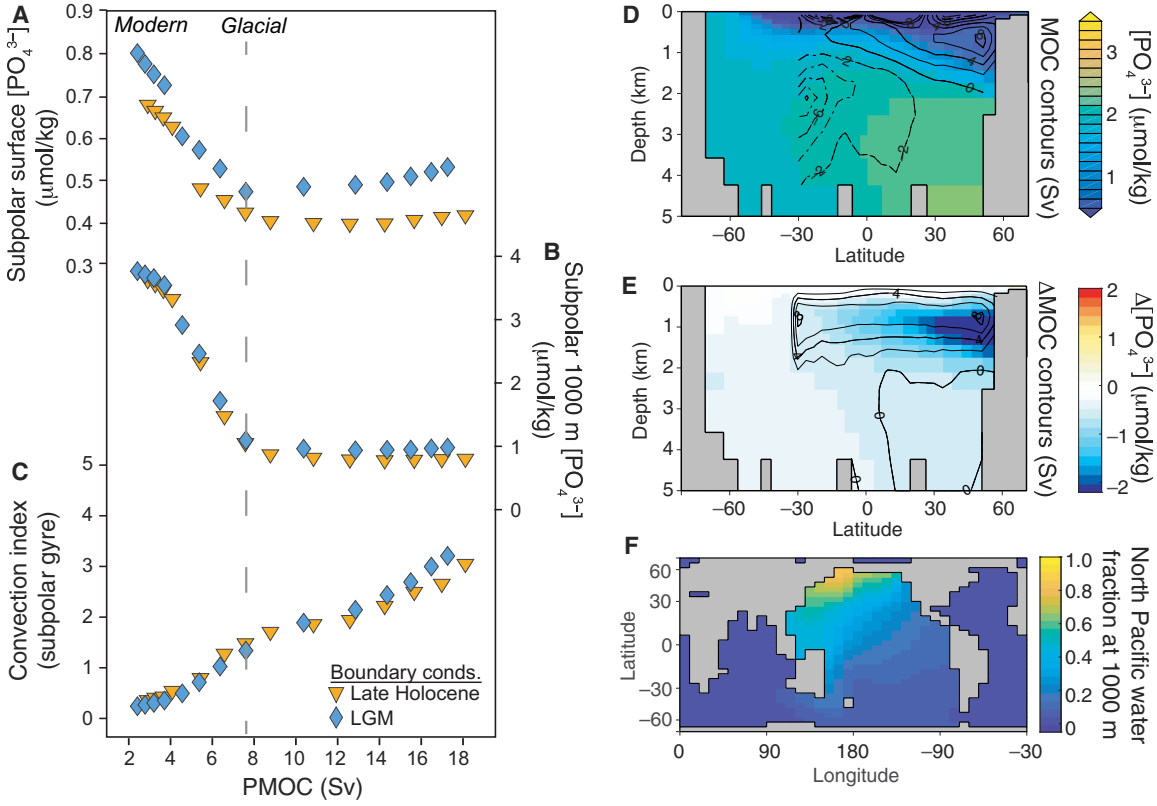

Fig. 4. cGENIE Earth system model experiments illustrating the impact of changes in North Pacific overturning on nutrient concentrations. Each symbol (**A** to **C**) represents a 5000-year-long model experiment under preindustrial (orange triangles) or glacial (blue diamonds) boundary conditions. Experiments are forced by decreasing the atmospheric freshwater flux into the North Pacific, which increases surface salinity and enhances PMOC (fig. S6). Output is plotted against the maximum meridional stream function in the North Pacific below 280 m. Phosphate concentrations are shown for (A) the surface layer (top 80 m) and (B) intermediate depths (928 to 1158 m) in the subpolar gyre (grid cells spanning 43°N to 66°N and 115°W to 225°W). Convection frequency (C), a count of convection events throughout the water column per model time step, is shown for the same region. Meridional sections of phosphate concentration (shading) at 165°W and Pacific meridional overturning stream function (contours) are shown in (**D**), for an experiment with a salinity forcing of −0.19 Sv and a PMOC of 8 Sv [indicated by a dashed line in (A) to (C)] that produces the best fit to our LGM data (Fig. 5 and fig. S10); anomalies of phosphate and overturning from the glacial base state are shown in (**E**); and the spread of North Pacific water at 1000-m depth, predominantly on the basin's western boundary, is shown in (**F**).

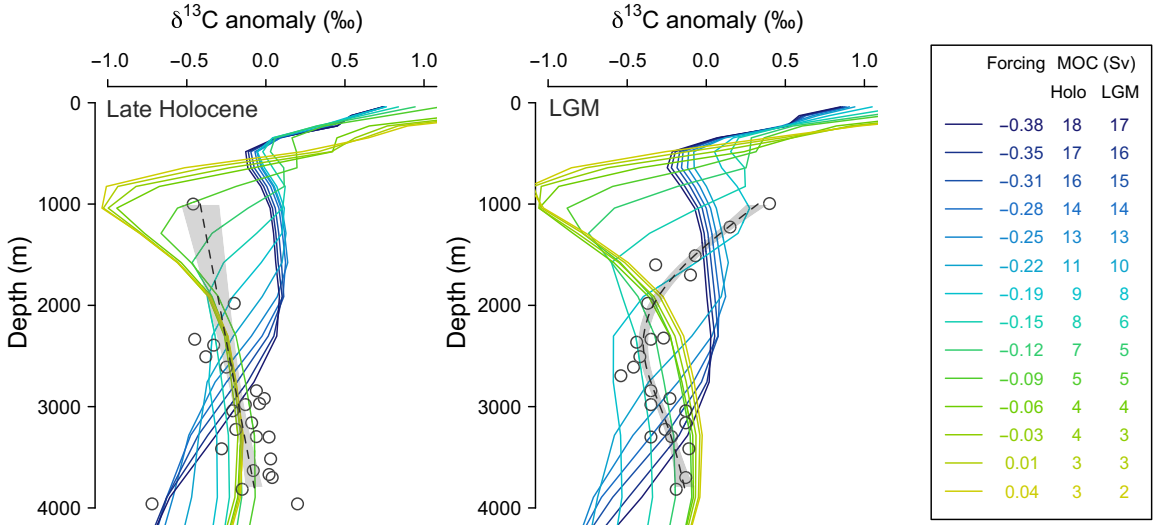

Fig. 5. Simulated $\delta^{13}C$ profiles in cGENIE compared to benthic $\delta^{13}C$ data in the NW Pacific. Data (*6*) are shown as symbols with a general additive model fit shown by the gray dashed line. cGENIE simulations are given by the colored lines. To aid comparison, all profiles are shown as $\delta^{13}C$ anomalies from the mean $\delta^{13}C$ for each profile. Left: Late Holocene data and the experiments run under preindustrial boundary conditions. Right: LGM data and experiments run under glacial boundary conditions. The legend lists the maximum North Pacific overturning for each experiment. The upper portion of the LGM $\delta^{13}C$ profile shows the closest match to the simulation run with an Atlantic to Pacific freshwater forcing of −0.19 Sv, which has a PMOC of 8 Sv. As the lower portions of the profiles likely remain ventilated by Southern Ocean waters, and as we have not made any changes to the Southern Ocean in our simulations, some offset at depth is to be expected.

glaciation ~2.7 million years ago (*14*) could be explained by increased PMOC, analogous to the change from modern to LGM conditions. We note that, as a transient condition, the onset of deep-water formation can lead to a short-lived peak in surface nutrients and CO_2, as convection initially taps into high-nutrient subsurface waters before they have been replaced with well-ventilated low-nutrient waters (fig. S9); this remains a likely explanation for North Pacific pH, $\delta^{13}C$, and ^{14}C excursions (*12*) during Heinrich Stadial 1 (HS1; ~17.5 to 16.0 ka). However, the typical pattern under steady-state conditions—both in paleo records and our modeling—appears to be that increased overturning drives a decrease in nutrient supply (Fig. 4).

The dynamics of a glacial PMOC

Increased ventilation of the North Pacific at the LGM would be facilitated by an increase in the salinity of subpolar surface waters (*2*, *3*), as implied by the available data (Fig. 2D and fig. S4). Higher salinity in the glacial North Pacific may be driven by reduced net precipitation (*P*-*E*), due to a weakened hydrological cycle under globally cooler conditions (*30*), and a southward shift in storm track precipitation (*31*). Increased Ekman suction in the presence of the Laurentide ice sheet (*29*) would also bring up salt from subsurface waters. Salinity may be further elevated by increased exchange with the saltier subtropical gyre, due to an intensification of the westerly winds in response to the Laurentide ice sheet (*22*, *29*), or as a Stommel feedback to an initial increase in overturning (*32*). Although an increase in SST would, in isolation, decrease the density of surface waters, this may be overcome by an increase in salinity, in part resulting from enhanced evaporation and divergent moisture transport (*2*); the combination of increased SST and increased North Pacific ventilation is indeed found in ocean circulation models (figs. S7 and S11). Last, it is possible that seasonal sea ice formation and brine rejection play a role (*8*, *25*), in particular, in helping to set the local sites of downwelling, which are likely to be in the marginal seas (*10*). Enhanced sea ice production may be reconciled with warmer SSTs either by a difference in seasonality or if sea ice production occurs predominantly in coastal settings (*8*). Although basin geometry and a closed Bering Strait may, in part, limit salinity in the North Pacific (*4*), our proxy reconstructions show that local ventilation to intermediate depths is indeed possible, a result also found in the higher-resolution NCAR CCSM3 and GFDL CM2Mc models under some instances of colder climate conditions (figs. S11 and S12).

Comparing reconstructed $\delta^{13}C$ profiles and other ventilation data with cGENIE output (Fig. 5 and fig. S10) suggests a PMOC of around 8 Sv at the LGM, which is also consistent with the changes seen in SST (fig. S7). Note, however, that the PMOC cell remains largely above 2000 m and within the Pacific basin in our cGENIE experiments (fig. S7), in contrast with Atlantic Meridional Overturning Circulation (AMOC) at similar overturning rates. $\delta^{13}C$ values in the intermediate North Pacific also remain lower than those in the glacial North Atlantic (fig. S13). These observations may, in part, be explained by the much greater volume of the Pacific, which increases the residence time of northern-sourced waters within the basin, and allows remineralization and mixing with southern-sourced waters to exert greater influence. While glacial AMOC may have remained higher than PMOC, the LGM's overturning circulation, with northern-fed cells in both basins to ~2000 m overlying southern-sourced waters, was substantially more symmetrical than today. It is possible that this more symmetrical glacial circulation is the most common configuration of the overturning circulation during the late Pleistocene, with today's asymmetric mode limited to peak interglacial conditions.

Impact of PMOC on CO_2

Enhanced PMOC would have increased the North Pacific's influence on the glacial carbon cycle and climate (Fig. 6). Today, the North Pacific is a High Nutrient Low Chlorophyll zone, with an

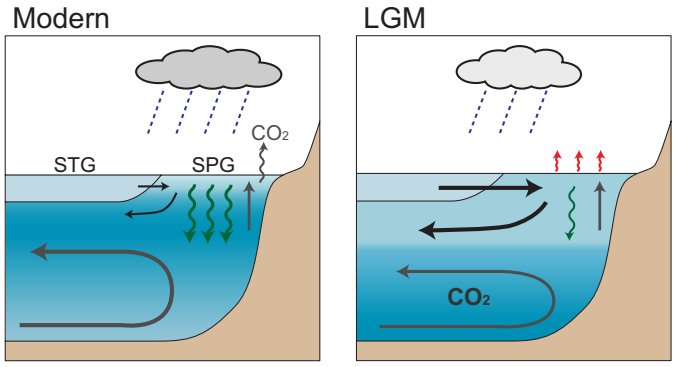

Fig. 6. Schematic of ocean circulation and productivity in the modern and LGM North Pacific. The modern North Pacific (**left**) lacks vigorous local ventilation (thin black arrows), because of low salinity in surface waters of the subpolar gyre (SPG). This is a result of high net precipitation (*P-E*) and minimal exchange with the saltier waters of the subtropical gyre (STG). The modern subpolar North Pacific is thus dominated by upwelling of nutrient- and CO_2-rich subsurface waters (gray vertical arrow), driving relatively high export productivity (green wavy arrows) and CO_2 outgassing. During the LGM (**right**), our data compilation suggests that ventilation at intermediate depths was enhanced, export productivity was reduced, and subpolar surface waters were saltier and warmer (red wavy arrows). This is consistent with an invigorated meridional overturning circulation, with enhanced formation of intermediate waters and advection of warm, salty, and nutrient-depleted subtropical waters to high latitudes, analogous to a shallower version of the overturning circulation seen in the modern North Atlantic.

inefficient biological pump and high CO_2 outgassing. By reducing the carbon content of the high-latitude North Pacific, an invigorated PMOC would have helped stem this CO_2 leak, as indicated by boron isotope data, which show LGM surface ocean CO_2 close to equilibrium with the atmosphere (*29*). Furthermore, these changes in the surface ocean would have had a greater impact on the net ocean CO_2 storage, because enhanced intermediate water formation would lower the preformed nutrient content of the ocean's interior. Combining our cGENIE results with a simple scaling between preformed phosphate and atmospheric CO_2 (*33*) shows that atmospheric CO_2 is relatively sensitive to modest increases in PMOC and suggests CO_2 drawdown on the order of ~16 parts per million (ppm) (see Materials and Methods and fig. S14). CO_2 drawdown may be further enhanced by PMOC's impact on biogeochemistry in the Southern Ocean (*34*). Today, carbon-rich waters recirculated from the Pacific upwell in the Southern Ocean and contribute to high surface nutrients and CO_2 outgassing in this region. Replacing a portion of this upwelling water with well-ventilated glacial NPIW reduces the carbon and nutrient supply to the Southern Ocean surface (see Earth system model results in fig. S8), thus increasing the efficiency of the Southern Ocean biological pump and further lowering atmospheric CO_2. This process may help explain the similarity in nutrient utilization records from the North Pacific and Southern Oceans [the "polar twins" (*35*)]. If enhanced glacial PMOC results from increased sea ice and ice sheet size, then this would provide a feedback between Northern Hemisphere insolation and atmospheric CO_2, linking the orbital pacing of the ice ages to global glacial climate change.

Regional warming in Beringia due to enhanced PMOC

The relatively mild regional climate supported by heat transport from an enhanced PMOC may have implications for the first human migration to the Americas. Recent genetic studies suggest that the founding population of early Native North and South Americans were isolated from other, future Asian populations during the LGM, before dispersing into and through the American continents (*16*). This isolation is thought to have been located in northeastern Siberia or on the now submerged Bering Sea shelf, lasting between 7000 and 15,000 years (*36*) during what is known as the "Beringian standstill." Some terrestrial records support the interpretation that this region was an ecological refugium, with spruce, birch, and alder pollen and fossil insects providing evidence of a relatively mild and maritime climate (*37*). However, given the extremely cold conditions further inland (*38*), it has remained unclear how habitable conditions could have been maintained. Our data and modeling suggest that an enhanced overturning circulation helped warm this region at the LGM, countering the influence of lower greenhouse gasses and higher albedo, to bring Pacific Beringian temperatures up to, or even warmer than, modern (Fig. 2C and figs. S1C and S4). Warming may have been particularly enhanced during LGM winters, as seen in CCSM3 (fig. S11B), which shows that for a mean annual temperature change of ~2°C in the glacial northwest Pacific (similar to our reconstructions), winter warming may have been around 6°C. An enhanced Pacific overturning circulation could have thus aided human habitation in Beringia during a period of refuge before migration to North America.

MATERIALS AND METHODS

Ventilation data

Sediment core proxy data for ventilation at the LGM includes $\delta^{13}C$ data on benthic foraminifera, tracers of sedimentary redox, and radiocarbon age offsets between benthic and planktic foraminifera, taken from sites above 20°N in the North Pacific (with a version above 40°N shown in fig. S1A). Stable carbon isotope data ($\delta^{13}C$) (*6*, *9*, *11*, *39*–*53*) on benthic foraminifera of the genus *Cibicides* are largely taken from the recent synthesis by Peterson *et al.* (*17*), supplemented with recent studies (*9*, *53*). Where possible, we compare foraminiferal data for the LGM (19 to 23 ka) and late Holocene (0 to 6 ka). At sites where Holocene foraminiferal data are not available (24 of 62), we use seawater $\delta^{13}C$ data taken from the PACIFic ocean Interior CArbon (PACIFICA) database (*52*), with values interpolated for these core sites using the three-dimensional estimation tool in Ocean Data View [ODV, (*54*)], except at Keigwin's (*6*) depth transect in the NW Pacific and Max's (*9*, *53*) sites in the Bering Sea, where we use the accompanying water column measurements. Both approaches show an increase in $\delta^{13}C$ at intermediate depths. To account for whole-ocean change in $\delta^{13}C$ at the LGM (attributed to a smaller terrestrial biosphere), and thus better reveal patterns of change in circulation, we correct LGM $\delta^{13}C$ values by +0.34‰ (*17*). We then calculate the LGM minus Holocene $\delta^{13}C$ difference, with positive values indicating higher $\delta^{13}C$ and increased ventilation at the LGM. We use a threshold value of ±0.1‰ for a significant increase/decrease in $\delta^{13}C$ when comparing LGM and Holocene foraminiferal data, based on 1 SD of replicate samples of benthic foraminifera from the NW Pacific (*6*). When comparing LGM foram $\delta^{13}C$ to modern water $\delta^{13}C$, we use a threshold value of 0.2‰, to account for calibration error [e.g., (*42*)] and the sparseness of water column $\delta^{13}C$ data in this region.

Redox reconstructions (*55*–*79*) follow the approach and compilation of Jaccard and Galbraith (*7*), who estimated whether oxygen

concentrations increased or decreased at the LGM (defined in their study to be 20 to 22 ka) compared to Holocene (5 to 10 ka). Redox proxies include trace metals, sediment laminations, assemblages of benthic foraminifera, and nitrogen isotopes from regions of modern denitrification. Following Jaccard and Galbraith (*7*), redox changes based on nitrogen isotopes are plotted at 400 m to reflect the depth of water column denitrification. We use the published thresholds for significant change in redox, quoted as approximately 1 SD.

Radiocarbon data (*12*, *20*, *53*, *70*, *76*, *80*–*100*) are taken largely from syntheses by (*13*, *18*–*20*). Glacial data shown in Fig. 2A consist of ^{14}C age offsets between benthic and planktic foraminifera from the same sample and include data with calendar ages in the window 18 to 23 ka. Holocene benthic-planktic ^{14}C data are rare in this region because of poor carbonate preservation, so we compare LGM benthic-planktic offsets to deep-surface offsets in water column ^{14}C. These are calculated from nearby deep-water ^{14}C data from GLODAPv2 (*101*) and a surface water age of 400 ^{14}Cyr south of the subpolar gyre boundary (43°N) and 700 ^{14}Cyr within the subpolar gyre. The threshold for a significant change at the LGM is the quadratic combination of ^{14}Cyr 1-SE measurement uncertainties on LGM benthic and planktic ^{14}C data and a 200-^{14}Cyr uncertainty on modern deep-surface offsets, and averages 289 ^{14}Cyr. The section view in Fig. 3C uses the datasets listed above with benthic data shown as age offsets from the contemporaneous atmosphere (*102*). Note that despite their varying influences and sources of uncertainty, each set of ventilation proxy data shows the same patterns of change at the LGM, with enhanced ventilation at intermediate depths and reduced ventilation in the abyss.

Productivity data

Biogenic opal and barium data (*26*, *59*, *74*, *76*, *87*, *103*–*118*) were taken from the compilation of Kohfeld and Chase (*26*) and supplemented with recent data from (*12*, *15*, *87*, *119*–*122*). LGM and Holocene mean values and SEs were calculated from data in the time windows 0 to 10 ka (Holocene) and 19 to 23 ka (LGM). A significant change is noted when the difference between the LGM and Holocene means exceeds the quadratic sum of their 1-SE values. Sedimentary opal (%) and barium (ppm) content are shown in Fig. 2B. Where available, published mass accumulation rate estimates of these biogenic components are shown in fig. S1B, largely based on sediment core age models (from δ^{18}O and ^{14}C) and dry bulk density (either measured or estimated); fluxes based on ^{230}Th are indicated with bold symbol outlines (fig. S1B). Each of these treatments of the data indicates reduced export productivity in the LGM subpolar North Pacific.

Temperature and salinity data

Published records of planktic foraminiferal Mg/Ca and $\delta^{18}O_{calcite}$ (*24*, *29*, *82*, *87*, *123*–*127*), $U^{K'}_{37}$ (*112*, *113*, *128*–*135*) covering the Holocene (0 to 10 ka) and LGM (19 to 21 ka) were collated for the North Pacific, spanning both the subpolar and subtropical gyres. All age models are as given in the original publication. All Mg/Ca were recalibrated (see below). $U^{K'}_{37}$ temperatures are as given in the original publication. For both Mg/Ca and $U^{K'}_{37}$, temperature change during the LGM is given as a difference to proxy-derived temperature in the Holocene.

We recalibrated the published Mg/Ca data using the "MgCaRB" approach, as detailed in (*136*), which accounts for changes in the nonthermal influences of salinity and pH downcore. For *Globigerinoides ruber* and *Globigerina bulloides*, we use the species-specific equations from (*136*). For *Neogloboquadrina pachyderma*, we use the species-specific sensitivities given in (*137*), which we incorporate into the MgCaRB protocol (note that *N. pachyderma* Mg/Ca appears insensitive to pH). While the direct temperature sensitivity of Mg/Ca in planktic foraminifera is ~6%/°C (*136*), because of the effect of temperature on pH through the disassociation constant of water (K_w), the "apparent" Mg/Ca temperature sensitivity is higher in pH-sensitive species (*138*). The MgCaRB approach accounts for the mean changes in surface salinity (due to sea level) and pH (due to atmospheric CO_2) downcore, iteratively solving Mg/Ca and pCO_2 to overcome the covariance induced by the thermal effect on K_w. Our approach does not account for local changes in salinity/pH; however, as local salinity and pH changes in both increase during the LGM, their effects on Mg/Ca work against each other, such that the bias on reconstructed temperature are likely to be small (a local 1–practical salinity unit (PSU) salinity and 0.05–pH unit increase would sum to zero temperature bias). Dissolution can also affect foraminiferal Mg/Ca, although this influence is thought to be relatively minor in lower-Mg planktic foraminifera such as *N. pachyderma* (*139*), the species analyzed most frequently in the high latitudes. LGM-Holocene changes in bottom water carbonate ion concentration are also relatively minor within the deep Pacific, decreasing by ~10 μmol kg^{-1}) during the LGM (*140*). Hence, although dissolution is unlikely to have a significant influence on changes in SST calculated from changes in Mg/Ca, the slight decrease in glacial bottom water carbonate ion concentration within the Pacific (*140*) would result in an apparent cooling in Mg/Ca SSTs. If we consider the sign of change in the secondary influences on Mg/Ca (local salinity, pH, and dissolution) from Holocene to LGM, then the warming signal that we see in Mg/Ca SSTs during the LGM is likely to be a conservative estimate; hence, the increase in ice volume–corrected seawater δ^{18}O (salinity) that we see is also likely to be a conservative estimate. For $U^{K'}_{37}$, the change in temperature at each site was calculated using the calibrations given in the original publications (*141*, *142*); the temperature range in this study is too low to be significantly influenced by the nonlinearity of $U^{K'}_{37}$ at >~24° (*143*).

The change in ice volume–corrected δ^{18}O of seawater ($\delta^{18}O_{sw\text{-}ivc}$) was calculated from samples with paired measurements of Mg/Ca and $\delta^{18}O_{calcite}$. We use the change in temperature calculated from the Mg/Ca values (described above) and the temperature-δ^{18}O fractionation factor of (*144*) to remove the temperature signal from $\delta^{18}O_{calcite}$. The effect of sea level was accounted for using the whole-ocean glacial $\delta^{18}O_{sw}$ change of 1‰ (*145*) scaled to the sea level record of (*146*). Note that the ice volume correction on δ^{18}O accounts for the fact that whole-ocean salinity was higher at the LGM; thus, an increase in $\delta^{18}O_{sw\text{-}ivc}$ represents an increase in salinity beyond the whole-ocean salinity increase.

We calculate the change in temperature and $\delta^{18}O_{sw\text{-}ivc}$ between the Holocene (0 to 10 ka) and LGM (19 to 21 ka) time slices for each record individually, with the change in temperature defined against the average for the Holocene. For five sites, we use the interval 0 to 11.5 ka for the Holocene and/or 17.9 to 21 ka for the LGM, and these sites are marked with a gray outline in Fig. 2C and fig. S1C; excluding these sites makes no difference to any of the conclusions drawn. We note that the use of data of early Holocene (which is relatively warm compared to the late Holocene and preindustrial; fig. S4) (*147*) within our Holocene time window means that the estimate of

LGM warming is again likely to be conservative. An increase/decrease is indicated by a change of >±1°C for Mg/Ca, >±1.2°C for $U^{K'}_{37}$, and >±0.25‰ for $\delta^{18}O_{sw\text{-}ivc}$. These thresholds correspond to the uncertainties associated with the temperature proxies (*136*, *141*, *142*) and the equivalent in $\delta^{18}O$ (*144*).

Time windows

Our data compilations take advantage of available syntheses of data from the North Pacific where available, supplemented with recently published data. Time slices selected for the LGM in these syntheses, as detailed above, are fairly consistent. Holocene time slices show more variety although, in each case, aim to most accurately represent postglacial Holocene conditions. For $\delta^{13}C$, this requires that the glacial-interglacial whole-ocean/atmosphere/biosphere change is complete, which was only achieved in the late Holocene. For some redox proxies, core-top values are liable to disturbance, so an early Holocene slice may be more appropriate. Late Holocene carbonate preservation in the North Pacific is poor, limiting Holocene proxy records based on planktic foraminifera. As a result, LGM benthic-planktic ^{14}C data are compared to modern values from the water column. Last, as noted above, the use of early Holocene data within our LGM to Holocene temperature comparison is likely to underestimate the magnitude of LGM warming compared to preindustrial, given the warmth of the early Holocene (*147*), so the LGM warming signal seen in Fig. 2C and figs. S1C and S4 is likely to be conservative. We also provide a $\delta^{13}C$ profile for a time slice ~3000 years older than the original LGM pick in fig. S2, which demonstrates that the enhanced ventilation signal is robust to age model uncertainties, and cannot be attributed to aliasing of an HS1 signal.

Box model

We use an adaptation of Warren (*2*) and Emile-Geay *et al.*'s (*3*) salinity budget for the North Pacific subpolar gyre to explore controls on salinity and nutrients in this region. The model considers a mass balance for water in a subpolar gyre box, representing latitudes 43°N to 63°N, longitudes 140°E to 120°W, and water depth 0 to 200 m, with inputs from the subtropical gyre (V_{STG}), upwelling (V_{UP}), net precipitation (*P-E*), and riverine runoff (*R*). Salinity of the subpolar gyre (S_{SPG}) is calculated from the ratio of inputs of salt to inputs of water

$$S_{SPG} = \frac{S_{UP} V_{UP} + S_{STG} V_{STG}}{V_{UP} + V_{STG} + (P - E) + R}$$

and depends on the salinity of subtropical input (S_{STG}) and upwelling water (S_{UP}). For the derivation of this equation, see (*2*) and (*3*). We follow the same approach to model phosphate concentration in the subpolar gyre ($PO_4^{3-}{}_{SPG}$)

$$PO_4^{3-}{}_{SPG} = \frac{PO_4^{3-}{}_{UP} V_{UP} + PO_4^{3-}{}_{STG} V_{STG}}{V_{UP} + V_{STG} + (P - E) + R}$$

using the volume transport terms and box definitions as described above and substituting salinity for phosphate concentrations in the subtropics ($PO_4^{3-}{}_{STG}$) and in upwelled waters ($PO_4^{3-}{}_{UP}$). Note that this formulation considers only phosphate supply by ocean advection and does not attempt to model removal by productivity. As a result, our modeled phosphate concentrations are equivalent to winter values before significant drawdown in the spring bloom.

We use Emile-Geay's (*3*) estimates of advective transport from the subtropical gyre and upwelling, Wills and Schneider's (*148*) estimates of *P-E* and R (taken from ERA-Interim reanalysis), and salinity and phosphate concentrations for subtropical and upwelled waters from World Ocean Atlas, computed using the box averaging tool in Ocean Data View (*149*). Following Warren (*2*), we consider only advection and do not attempt to account for the influence of diffusion or eddy flux, which have large uncertainties for salinity and are poorly constrained for phosphate. We checked this assumption with an estimate of phosphate eddy flux, based on the eddy transport terms determined by Emile-Geay (*3*) for salinity and using regional phosphate gradients. This made little difference (<5%) to our results, as the resulting values were small, and the supply of phosphate by vertical eddy flux is countered by the influence of nutrient-poor water from horizontal eddy flux. We use Warren's approach (*2*) to obtain subtropical and upwelling salinity and phosphate values with minimal influence from eddy exchange with water from the subpolar gyre, by excluding values immediately adjacent to the subpolar gyre. Our subtropical surface values use a box spanning 24°N to 40°N, 135°E to 115°W, and depths 0 to 200 m, and our upwelling values are taken from 2000 m, with the same latitude and longitude bounds as the surface subpolar box. All model input values are given in table S2.

The model accurately reproduces the salinity of the modern North Pacific subpolar gyre (33.0). The model gives phosphate in the subpolar gyre of 2.0 μmol/kg, slightly higher than annual average values of 1.8 μmol/kg in the modern North Pacific, but matching February (prespring bloom) values of 2.0 μmol/kg. The influence of possible glacial conditions is shown in fig. S5 and table S1. Subpolar salinity increases when (i) net precipitation is reduced, (ii) upwelling is increased, and (iii) exchange with the subtropics is enhanced, particularly when subtropical salinity is elevated. Phosphate concentrations in the subpolar gyre are reduced by exchange with the subtropics and by decreasing the phosphate concentrations of upwelled waters and are increased by increasing the upwelling flux. However, the increase in the upwelling flux has less impact on surface phosphate than the reduction of the phosphate concentration of the upwelled water; indeed, the net effect of doubling vertical exchange while halving subsurface nutrients is similar to that of halving subsurface nutrients alone (fig. S5). Because the wind- and tidally driven transfer of water from the subsurface to the surface North Pacific is high, vertical nutrient gradients are relatively low, so further increase in vertical exchange (e.g., with reduced stratification) has less influence than decreasing the nutrient content of the upwelled water, as a result further substantiated by Earth system modeling (see below).

cGENIE Earth system model

To explore the impact of enhanced North Pacific overturning on nutrients and tracers in more detail, we ran a series of sensitivity tests with the "muffin" release of the cGENIE Earth system model (*150*). cGENIE consists of a three-dimensional frictional geostrophic ocean circulation model, two-dimensional sea ice and energy-moisture balance atmospheric models and incorporates representations of the marine geochemical cycling of carbon and other biologically mediated tracers (*151*). We use cGENIE with a 36 × 36 equal-area horizontal resolution and 16 vertical levels, with highest vertical resolution toward the ocean surface. Ocean physics and carbon cycle configuration are as described and evaluated in (*150*), with the addition of iron colimitation on marine productivity (*152*). Despite its coarse resolution, cGENIE successfully reproduces

many of the large-scale features of marine biogeochemical cycles in the present-day (*150*, *151*). Of particular relevance to this study, cGENIE predicts nutrient (PO_4^{3-}) distributions in the North Pacific that are in agreement with present-day observations (*151*). The coarse resolution also allows cGENIE to be run efficiently and a broad parameter space to be explored: here, we show 28 × 5000–year runs for two sets of boundary conditions.

To test the potential influence of background climate state on our results, we ran experiments under preindustrial and glacial boundary conditions. To simulate a glacial climate state, we reduced the radiative forcing consistent with concentrations of the major greenhouse gases (CO_2, CH_4, and N_2O of 191 ppm, 350 parts per billion (ppb), and 216 ppb, respectively; *153*–*155*). In addition, we increased the zonally averaged planetary albedo profile in the Northern Hemisphere and increased average ocean salinity by ~1 PSU, similar to that used in (*12*). Our experiments start from the end of 20,000-year equilibrium spin-ups carried out with prescribed atmospheric CO_2 of 278 ppm, $\delta^{13}C$ of −6.50‰, and $\Delta^{14}C$ of 0‰. The same prescribed atmospheric CO_2 concentration and isotopic compositions are used for both preindustrial and glacial boundary conditions, so that the size of the ocean-atmosphere carbon inventory is similar across our experiments. Radiative forcing by CO_2 is set independently of the actual concentration of atmospheric CO_2 calculated by the ocean-atmosphere biogeochemistry modules and is held constant at either preindustrial or glacial levels as described above.

To simulate an increase in North Pacific ventilation, we reduced the prescribed transfer of atmospheric fresh water from the Atlantic to the Pacific, which implicitly accounts for the net moisture transport between these basins (*156*, *157*). We ran 28 total experiments under preindustrial and glacial boundary conditions, with a range of freshwater transport anomalies from 0.04 to −0.38 Sv. Experiments were run for 5000 years, which allows ocean circulation and nutrient concentrations to stabilize, with <2% change in mean global surface PO_4^{3-} over the last 500 years of the simulations.

The decrease in atmospheric freshwater transport from the Atlantic to the Pacific increases PMOC and reduces AMOC. The redistribution of surface salinity also changes deep-water formation in the Southern Ocean, in turn changing biological pump efficiency. Each of these processes may change atmospheric CO_2, and deconvolving their individual influences is beyond the scope of this study. To place broad constraints on changes in pCO_2 due to enhanced PMOC, we calculate changes in the ocean's preformed phosphate inventory resulting from increased input of NPIW and use the theoretical scaling of Ito and Follows (*33*) to estimate the pCO_2 impact. We use a dye tracer to calculate the volumetric contribution of North Pacific waters to the ocean's interior and use the end-member preformed phosphate composition of the grid box with the maximum contribution of NPIW. We assume that this NPIW replaces water in the Pacific's interior that has a preformed phosphate of 1.4 μmol/kg (*158*) and calculate the resulting difference in preformed phosphate inventory by mass balance. The results of this mass balance calculation are shown in fig. S14, with contours showing the general relationship between NPIW volume, preformed phosphate, and pCO_2 change, and symbols showing the realizations found in our cGENIE simulations. With enhanced PMOC, the preformed phosphate content of NPIW decreases, as nutrients are flushed from the subpolar gyre, and this low-phosphate water occupies a greater ocean volume, thus increasing the net efficiency of the biological pump and decreasing atmospheric CO_2. To estimate the cGENIE scenario most representative of LGM conditions in the North Pacific, we compare modeled $\delta^{13}C$ profiles in the NW Pacific to the data (Fig. 5 and fig. S10). An overturning rate of 8 Sv, found with an Atlantic to Pacific freshwater forcing anomaly of −0.19 Sv, best matches the shape of the LGM $\delta^{13}C$ profile (Fig. 5) and also shows a good match to observed changes in $\delta^{13}C$, redox, and ^{14}C across the basin (fig. S10). We thus estimate a change in pCO_2 of ~16 ppm as a result of enhanced PMOC at the LGM. However, we note that the influence of changes in ocean circulation and preformed nutrient inventory on pCO_2 may vary depending on circulation regime in the Southern Ocean (*34*), and that other processes, including sea ice and carbonate compensation, will also influence CO_2 but are not captured by this treatment. Further work is required to constrain the impact of PMOC on pCO_2 in more detail.

SUPPLEMENTARY MATERIALS

Supplementary material for this article is available at http://advances.sciencemag.org/cgi/content/full/6/50/eabd1654/DC1

REFERENCES AND NOTES

1. D. M. Sigman, M. P. Hain, G. H. Haug, The polar ocean and glacial cycles in atmospheric CO2 concentration. *Nature* **466**, 47–55 (2010).
2. B. A. Warren, Why is no deep water formed in the North Pacific? *J. Mar. Res.* **41**, 327–347 (1983).
3. J. Emile-Geay, M. A. Cane, N. Naik, R. Seager, A. C. Clement, A. van Geen, Warren revisited: Atmospheric freshwater fluxes and "why is no deep water formed in the North Pacific". *J. Geophys. Res.* **108**, 3178 (2003).
4. D. Ferreira, P. Cessi, H. K. Coxall, A. de Boer, H. A. Dijkstra, S. S. Drijfhout, T. Eldevik, N. Harnik, J. F. McManus, D. P. Marshall, J. Nilsson, F. Roquet, T. Schneider, R. C. Wills, Atlantic-Pacific asymmetry in deep water formation. *Annu. Rev. Earth Planet. Sci.* **46**, 327–352 (2018).
5. J. L. Sarmiento, N. Gruber, M. A. Brezinski, J. P. Dunne, High-latitude controls of thermocline nutrients and low latitude biological productivity. *Nature* **427**, 56–60 (2004).
6. L. D. Keigwin, Glacial-age hydrography of the far northwest Pacific Ocean. *Paleoceanography* **13**, 323–339 (1998).
7. S. L. Jaccard, E. D. Galbraith, Large climate-driven changes of oceanic oxygen concentrations during the last deglaciation. *Nat. Geosci.* **5**, 151–156 (2011).
8. K. P. Knudson, A. C. Ravelo, North Pacific Intermediate Water circulation enhanced by the closure of the Bering Strait. *Paleoceanography* **30**, 1287–1304 (2015).
9. L. Max, N. Rippert, L. Lembke-Jene, A. Mackensen, D. Nürnberg, R. Tiedemann, Evidence for enhanced convection of North Pacific Intermediate Water to the low-latitude Pacific under glacial conditions. *Paleoceanography* **32**, 41–55 (2016).
10. M. S. Cook, A. C. Ravelo, A. Mix, I. M. Nesbitt, N. V. Miller, Tracing subarctic Pacific water masses with benthic foraminiferal stable isotopes during the LGM and late Pleistocene. *Deep Sea Res. II Topical Stud. Ocean.* **125–126**, 84–95 (2016).
11. K. Matsumoto, T. Oba, J. Lynch-Stieglitz, H. Yamamoto, Interior hydrography and circulation of the glacial Pacific Ocean. *Quat. Sci. Rev.* **21**, 1693–1704 (2002).
12. J. W. B. Rae, M. Sarnthein, G. L. Forster, A. Ridgwell, P. M. Grootes, T. Elliot, Deep water formation in the North Pacific and deglacial CO_2 rise. *Paleoceanography* **29**, 645–667 (2014).
13. Y. Okazaki, A. Timmermann, L. Menviel, N. Harada, A. Abe-Ouchi, M. O. Chikamoto, A. Mouchet, H. Asahi, Deepwater formation in the North Pacific during the last glacial termination. *Science* **329**, 200–204 (2010).
14. D. M. Sigman, S. L. Jaccard, G. H. Haug, Polar ocean stratification in a cold climate. *Nature* **428**, 59–63 (2004).
15. H. Ren, A. S. Studer, S. Serno, D. M. Sigman, Glacial-to-interglacial changes in nitrate supply and consumption in the subarctic North Pacific from microfossil-bound N isotopes at two trophic levels. *Biogeosciences* **30**, 1217–1232 (2015).
16. E. Tamm, T. Kivisild, M. Reidla, M. Metspalu, D. G. Smith, C. J. Mulligan, C. M. Bravi, O. Rickards, C. Martinez-Labarga, E. K. Khusnutdinova, S. A. Fedorova, M. V. Golubenko, V. A. Stepanov, M. A. Gubina, S. I. Zhadanov, L. P. Ossipova, L. Damba, M. I. Voevoda, J. E. Dipierri, R. Villems, R. S. Malhi, Beringian standstill and spread of Native American founders. *PLOS ONE* **2**, e829–e826 (2007).
17. C. D. Peterson, L. E. Lisiecki, J. V. Stern, Deglacial whole-ocean $\delta^{13}C$ change estimated from 480 benthic foraminiferal records. *Paleoceanography* **29**, 549–563 (2014).
18. N. Zhao, O. Marchal, L. Keigwin, D. Amrhein, G. Gebbie, A synthesis of deglacial deep-sea radiocarbon records and their (In)Consistency with modern ocean ventilation. *Paleoceanogr. Paleoclimatol.* **33**, 128–151 (2018).

19. L. C. Skinner, F. Primeau, E. Freeman, M. de la Fuente, P. A. Goodwin, J. Gottschalk, E. Huang, I. N. McCave, T. L. Noble, A. E. Scrivner, Radiocarbon constraints on the glacial ocean circulation and its impact on atmospheric CO_2. *Nat. Commun.* **8**, 16010 (2017).
20. L. D. Keigwin, S. J. Lehman, Radiocarbon evidence for a possible abyssal front near 3.1 km in the glacial equatorial Pacific Ocean. *Earth Planet. Sci. Lett.* **425**, 93–104 (2015).
21. D. C. Lund, J. F. Adkins, R. Ferrari, Abyssal Atlantic circulation during the Last Glacial Maximum: Constraining the ratio between transport and vertical mixing. *Paleoceanography* **26**, PA1213 (2011).
22. W. R. Gray, R. C. J. Wills, J. W. B. Rae, A. Burke, R. F. Ivanovic, W. H. G. Roberts, D. Ferreira, P. J. Valdes, Wind-driven evolution of the north pacific subpolar gyre over the last deglaciation. *Geophys. Res. Lett.* **47**, 208–212 (2020).
23. N. Harada, O. Seki, A. Timmermann, H. Moossen, J. Bendle, Y. Nakamura, K. Kimoto, Y. Okazaki, K. Nagashima, S. A. Gorbarenko, A. Ijiri, T. Nakatsuka, L. Menviel, M. O. Chikamoto, A. Abe-Ouchi, S. Schouten, Sea surface temperature changes in the Okhotsk Sea and adjacent North Pacific during the last glacial maximum and deglaciation. *Deep Sea Res. II Top. Stud. Oceanogr.* **61-64**, 93–105 (2012).
24. J.-R. Riethdorf, L. Max, D. Nürnberg, L. Lembke-Jene, R. Tiedemann, Deglacial development of (sub) sea surface temperature and salinity in the subarctic northwest Pacific: Implications for upper-ocean stratification. *Paleoceanography* **28**, 91–104 (2013).
25. M. Méheust, R. Stein, K. Fahl, R. Gersonde, Sea-ice variability in the subarctic North Pacific and adjacent Bering Sea during the past 25 ka: New insights from IP_{25} and $U^{k'}_{37}$ proxy records. *Ark. Dent.* **4**, 1–19 (2018).
26. K. E. Kohfeld, Z. Chase, Controls on deglacial changes in biogenic fluxes in the North Pacific Ocean. *Quat. Sci. Rev.* **30**, 3350–3363 (2011).
27. S. Serno, G. Winckler, R. F. Anderson, E. Maier, H. Ren, R. Gersonde, G. H. Haug, Comparing dust flux records from the Subarctic North Pacific and Greenland: Implications for atmospheric transport to Greenland and for the application of dust as a chronostratigraphic tool. *Paleoceanography* **30**, 583–600 (2015).
28. L. Menviel, M. H. England, K. J. Meissner, A. Mouchet, J. Yu, Atlantic-Pacific seesaw and its role in outgassing CO_2 during Heinrich events. *Paleoceanography* **29**, 58–70 (2014).
29. W. R. Gray, J. W. B. Rae, R. C. J. Wills, A. E. Shevenell, B. Taylor, A. Burke, G. L. Foster, C. H. Lear, Deglacial upwelling, productivity and CO_2 outgassing in the North Pacific Ocean. *Nat. Geosci.* **11**, 340–344 (2018).
30. I. M. Held, B. J. Soden, Robust responses of the hydrological cycle to global warming. *J. Climate* **19**, 5686–5699 (2006).
31. J. M. Lora, J. L. Mitchell, A. E. Tripati, Abrupt reorganization of North Pacific and western North American climate during the last deglaciation. *Geophys. Res. Lett.* **43**, 11796–11804 (2016).
32. H. Stommel, Thermohaline convection with two stable regimes of flow. *Tellus* **13**, 224–230 (1961).
33. T. Ito, M. J. Follows, Preformed phosphate, soft tissue pump and atmospheric CO_2. *J. Mar. Res.* **63**, 813–839 (2005).
34. M. P. Hain, D. M. Sigman, G. H. Haug, Carbon dioxide effects of Antarctic stratification, North Atlantic Intermediate Water formation, and subantarctic nutrient drawdown during the last ice age: Diagnosis and synthesis in a geochemical box model. *Global Biogeochem. Cycles* **24**, GB4023 (2010).
35. G. H. Haug, D. M. Sigman, Palaeoceanography: Polar twins. *Nat. Geosci.* **2**, 91–92 (2009).
36. K. E. Graf, I. Buvit, Human dispersal from Siberia to Beringia: Assessing a Beringian standstill in light of the archaeological evidence. *Curr. Anthropol.* **58**, S583–S603 (2017).
37. V. D. Meyer, J. Hefter, G. Lohmann, L. Max, R. Tiedemann, G. Mollenhauer, Summer temperature evolution on the Kamchatka Peninsula, Russian Far East, during the past 20 000 years. *Clim. Past* **13**, 359–377 (2017).
38. M. Melles, J. Brigham-Grette, P. S. Minyuk, N. R. Nowaczyk, V. Wennrich, R. M. De Conto, P. M. Anderson, A. A. Andreev, A. Coletti, T. L. Cook, E. Haltia-Hovi, M. Kukkonen, A. V. Lozhkin, P. Rosén, P. Tarasov, H. Vogel, B. Wagner, 2.8 million years of Arctic climate change from Lake El'gygytgyn, NE Russia. *Science* **337**, 315–320 (2012).
39. J. C. Herguera, T. Herbert, M. Kashgarian, C. Charles, Intermediate and deep water mass distribution in the Pacific during the Last Glacial Maximum inferred from oxygen and carbon stable isotopes. *Quat. Sci. Rev.* **29**, 1228–1245 (2010).
40. J. Lynch-Stieglitz, R. G. Fairbanks, C. D. Charles, Glacial-interglacial history of Antarctic Intermediate Water: Relative strengths of Antarctic versus Indian Ocean sources. *Paleoceanography* **9**, 7–29 (1994).
41. L. D. Stott, M. Neumann, D. Hammond, Intermediate water ventilation on the Northeastern Pacific Margin during the Late Pleistocene inferred from benthic foraminiferal $\delta^{13}C$. *Paleoceanography* **15**, 161–169 (2000).
42. J.-C. Duplessy, N. J. Shackleton, R. K. Matthews, W. Prell, W. F. Ruddiman, M. Caralp, C. H. Hendy, ^{13}C Record of benthic foraminifera in the last interglacial ocean: Implications for the carbon cycle and the global deep water circulation. *Quatern. Res.* **21**, 225–243 (1984).
43. D. H. Andreasen, M. Flower, M. Harvey, S. Chang, A. C. Ravelo, Data report: Late Pleistocene oxygen and carbon isotopic records from sites 1011, 1012, and 1018. *Proc. ODP Sci. Results* **167**, 141–144 (2000).
44. E. A. Boyle, Cadmium and $\delta^{13}C$ paleochemical ocean distributions during the stage 2 glacial maximum. *Annu. Rev. Earth Planet. Sci.* **20**, 245–287 (1992).
45. T. Oba, M. Murayama, M. Yamauchi, M. Yamane, S. Oka, H. Yamamoto, Oxygen isotopic ratio of foraminiferal tests in marine sediment cores collected during "Mirai" MR97-04 cruise. *JAMSTEC-R*, (1999).
46. M. Lyle, I. Koizumi, C. Richter, R. J. Behl, P. Boden, J.-P. Caulet, M. L. Delaney, P. deMenocal, M. Desmet, E. Fornaciari, A. Hayashida, F. Heider, J. Hood, S. A. Hovan, T. R. Janecek, A. G. Janik, J. Kennett, D. Lund, M. L. Machain C., T. Maruyama, R. B. Merrill, D. J. Mossman, J. Pike, A. C. Ravelo, G. A. Rozo Vera, R. Stax, R. Tada, J. Thurow, M. Yamamoto, Sites 1010 and 1011, in *Proceedings of the Ocean Drilling Program, Initial Reports*, R. N. Riegel, Ed. (Ocean Drilling Program, 1997), vol. 167, pp. 49–173.
47. C. Sancetta, M. Lyle, L. Heusser, R. Zahn, J. P. Bradbury, Late-glacial to holocene changes in winds, upwelling, and seasonal production of the northern California current system. *Quatern. Res.* **38**, 359–370 (1992).
48. University of Cambridge, "Delphi", https://www.esc.cam.ac.uk/images/research-images/research-group/research-projects/delphi.
49. L. Wang, M. Sarnthein, H. Erlenkeuser, J. Grimalt, P. Grootes, S. Heilig, E. Ivanova, M. Kienast, C. Pelejero, U. Pflaumann, East Asian monsoon climate during the Late Pleistocene: High-resolution sediment records from the South China Sea. *Mar. Geol.* **156**, 245–284 (1999).
50. S. A. Hovan, D. K. Rea, N. G. Pisias, Late Pleistocene continental climate and oceanic variability recorded in northwest Pacific sediments. *Paleoceanography* **6**, 349–370 (1991).
51. R. Zahn, A. Rushdi, N. G. Pisias, B. D. Bornhold, B. Blaise, R. Karlin, Carbonate deposition and benthic $\delta\,^{13}C$ in the subarctic Pacific: Implications for changes of the oceanic carbonate system during the past 750,000 years. *Earth Planet. Sci. Lett.* **103**, 116–132 (1991).
52. T. Suzuki, M. Ishii, M. Aoyama, J. R. Christian, K. Enyo, T. Kawano, R. M. Key, N. Kosugi, A. Kozyr, L. A. Miller, A. Murata, T. Nakano, T. Ono, T. Saino, K.-i. Sasaki, D. Sasano, Y. Takatani, M. Wakita, C. L. Sabine, PACIFICA Data Synthesis Project. (ORNL/CDIAC-159, 2013); 10.3334/CDIAC/OTG.PACIFICA_NDP092.
53. L. Max, L. Lembke-Jene, J.-R. Riethdorf, R. Tiedemann, D. Nürnberg, H. Kühn, A. Mackensen, Pulses of enhanced North Pacific Intermediate Water ventilation from the Okhotsk Sea and Bering Sea during the last deglaciation. *Clim. Past* **10**, 591–605 (2014).
54. R. Schlitzer, Ocean Data View (2010); http://odv.awi.de.
55. K. G. Cannariato, J. P. Kennett, Climatically related millennial-scale fluctuations in strength of California margin oxygen-minimum zone during the past 60 k.y. *Geology* **27**, 975–978 (1999).
56. T. S. Ivanochko, T. F. Pedersen, Determining the influences of Late Quaternary ventilation and productivity variations on Santa Barbara Basin sedimentary oxygenation: A multi-proxy approach. *Quat. Sci. Rev.* **23**, 467–480 (2004).
57. I. L. Hendy, T. F. Pedersen, Is pore water oxygen content decoupled from productivity on the California Margin? Trace element results from Ocean Drilling Program Hole 1017E, San Lucia slope, California. *Paleoceanography* **20**, PA4026 (2005).
58. W. E. Dean, Sediment geochemical records of productivity and oxygen depletion along the margin of western North America during the past 60,000 years: Teleconnections with Greenland Ice and the Cariaco Basin. *Quat. Sci. Rev.* **26**, 98–114 (2007).
59. A. S. Chang, T. F. Pedersen, I. L. Hendy, Late Quaternary paleoproductivity history on the Vancouver Island margin, western Canada: A multiproxy geochemical study. *Can. J. Earth Sci.* **45**, 1283–1297 (2008).
60. Y. Zheng, A. van Geen, R. F. Anderson, J. V. Gardner, W. E. Dean, Intensification of the northeast Pacific oxygen minimum zone during the Bölling-Alleröd warm period. *Paleoceanography* **15**, 528–536 (2000).
61. R. S. Ganeshram, T. F. Pedersen, S. E. Calvert, G. W. McNeill, M. R. Fontugne, Glacial-interglacial variability in denitrification in the world's oceans: Causes and consequences. *Paleoceanography* **15**, 361–376 (2000).
62. T. J. Nameroff, S. E. Calvert, J. W. Murray, Glacial-interglacial variability in the eastern tropical North Pacific oxygen minimum zone recorded by redox-sensitive trace metals. *Paleoceanography* **19**, PA1010 (2004).
63. R. J. Behl, J. P. Kennett, Brief interstadial events in the Santa Barbara basin, NE Pacific, during the past 60 kyr. *Nature* **379**, 243–246 (1996).
64. K. G. Cannariato, J. P. Kennett, R. J. Behl, Biotic response to late Quaternary rapid climate switches in Santa Barbara Basin: Ecological and evolutionary implications. *Geology* **27**, 63–66 (1999).
65. E. Emmer, R. C. Thunell, Nitrogen isotope variations in Santa Barbara Basin sediments: Implications for denitrification in the eastern tropical North Pacific during the last 50,000 years. *Paleoceanography* **15**, 377–387 (2000).
66. W. E. Dean, The geochemical record of the last 17,000 years in the Guaymas Basin, Gulf of California. *Chem. Geol.* **232**, 87–98 (2006).
67. H. Cheshire, J. Thurow, A. J. Nederbragt, Late Quaternary climate change record from two long sediment cores from Guaymas Basin, Gulf of California. *J. Quat. Sci.* **20**, 457–469 (2005).
68. T. M. Hill, J. P. Kennett, D. K. Pak, R. J. Behl, C. Robert, L. Beaufort, Pre-Bølling warming in Santa Barbara Basin, California: Surface and intermediate water records of early deglacial warmth. *Quat. Sci. Rev.* **25**, 2835–2845 (2006).

69. A. Shibahara, K. Ohkushi, J. P. Kennett, K. Ikehara, Late Quaternary changes in intermediate water oxygenation and oxygen minimum zone, northern Japan: A benthic foraminiferal perspective. *Paleoceanography* **22**, PA3213 (2007).
70. K. Ikehara, K. Ohkushi, A. Shibahara, M. Hoshiba, Change of bottom water conditions at intermediate depths of the Oyashio region, NW Pacific over the past 20,000 yrs. *Global Planet. Change* **53**, 78–91 (2006).
71. Y. Ishizaki, K. Ohkushi, T. Ito, H. Kawahata, Abrupt changes of intermediate-water oxygen in the northwestern Pacific during the last 27 kyr. *Geo-Mar. Lett.* **29**, 125–131 (2009).
72. O. Cartapanis, K. Tachikawa, E. Bard, Northeastern Pacific oxygen minimum zone variability over the past 70 kyr: Impact of biological production and oceanic ventilation. *Paleoceanography* **26**, PA4208 (2011).
73. M. Shigemitsu, H. Narita, Y. W. Watanabe, N. Harada, S. Tsunogai, Ba, Si, U, Al, Sc, La, Th, C and $^{13}C/^{12}C$ in a sediment core in the western subarctic Pacific as proxies of past biological production. *Mar. Chem.* **106**, 442–455 (2007).
74. Y. Okazaki, K. Takahashi, H. Asahi, K. Katsuki, J. Hori, H. Yasuda, Y. Sagawa, H. Tokuyama, Productivity changes in the Bering Sea during the late Quaternary. *Deep Sea Res. II Top. Stud. Oceanogr.* **52**, 2150–2162 (2005).
75. J. Crusius, T. F. Pedersen, S. E. Calvert, G. L. Cowie, T. Oba, A 36 kyr geochemical record from the Sea of Japan of organic matter flux variations and changes in intermediate water oxygen concentrations. *Paleoceanography* **14**, 248–259 (1999).
76. E. D. Galbraith, S. L. Jaccard, T. F. Pedersen, D. M. Sigman, G. H. Haug, M. Cook, J. R. Southon, R. Francois, Carbon dioxide release from the North Pacific abyss during the last deglaciation. *Nature* **449**, 890–893 (2007).
77. S. L. Jaccard, E. D. Galbraith, D. M. Sigman, G. H. Haug, R. Francois, T. F. Pedersen, P. Dulski, H. R. Thierstein, Subarctic Pacific evidence for a glacial deepening of the oceanic respired carbon pool. *Earth Planet. Sci. Lett.* **277**, 156–165 (2009).
78. E. D. Galbraith, M. Kienast, S. L. Jaccard, T. F. Pedersen, B. G. Brunelle, D. M. Sigman, T. Kiefer, Consistent relationship between global climate and surface nitrate utilization in the western subarctic Pacific throughout the last 500 ka. *Paleoceanography* **23**, PA2212 (2008).
79. S. S. Kienast, S. E. Calvert, T. F. Pedersen, Nitrogen isotope and productivity variations along the northeast Pacific margin over the last 120 kyr: Surface and subsurface paleoceanography. *Paleoceanography* **17**, 1055 (2002).
80. A. C. Mix, D. C. Lund, N. G. Pisias, P. Bodén, L. Bornmalm, M. Lyle, J. Pike, *Rapid Climate Oscillations in the Northeast Pacific During the Last Deglaciation Reflect Northern and Southern Hemisphere Sources* (Geophysical Monograph Series, American Geophysical Union, 1999), vol. 112.
81. J. P. Kennett, B. L. Ingram, A 20,000-year record of ocean circulation and climate change from the Santa Barbara basin. *Nature* **377**, 510–514 (1995).
82. T. Sagawa, K. Ikehara, Intermediate water ventilation change in the subarctic northwest Pacific during the last deglaciation. *Geophys. Res. Lett.* **35**, L24702 (2008).
83. N. Ahagon, K. Ohkushi, M. Uchida, T. Mishima, Mid-depth circulation in the northwest Pacific during the last deglaciation: Evidence from foraminiferal radiocarbon ages. *Geophys. Res. Lett.* **30**, 2097 (2003).
84. M. Hoshiba, N. Ahagon, K. Ohkushi, M. Uchida, I. Motoyama, A. Nishimura, Foraminiferal oxygen and carbon isotopes during the last 34 kyr off northern Japan, northwestern Pacific. *Mar. Micropaleontol.* **61**, 196–208 (2006).
85. M. S. Cook, L. D. Keigwin, Radiocarbon profiles of the NW Pacific from the LGM and deglaciation: Evaluating ventilation metrics and the effect of uncertain surface reservoir ages. *Paleoceanography* **30**, 174–195 (2015).
86. L. D. Keigwin, Late Pleistocene-Holocene paleoceanography and ventilation of the Gulf of California. *J. Oceanogr.* **58**, 421–432 (2002).
87. H. Gebhardt, M. Sarnthein, P. M. Grootes, T. Kiefer, H. Kuehn, F. Schmieder, U. Röhl, Paleonutrient and productivity records from the subarctic North Pacific for Pleistocene glacial terminations I to V. *Paleoceanography* **23**, PA4212 (2008).
88. S. A. Gorbarenko, J. R. Southon, L. D. Keigwin, M. V. Cherepanova, I. G. Gvozdeva, Late Pleistocene–Holocene oceanographic variability in the Okhotsk Sea: Geochemical, lithological and paleontological evidence. *Palaeogeogr. Palaeoclimatol. Palaeoecol.* **209**, 281–301 (2004).
89. D. C. Lund, A. C. Mix, J. Southon, Increased ventilation age of the deep northeast Pacific Ocean during the last deglaciation. *Nat. Geosci.* **4**, 771–774 (2011).
90. J.-C. Duplessy, M. Arnold, E. Bard, A. Juillet-Leclerc, N. Kallel, L. Labeyrie, AMS ^{14}C study of transient events and of the ventilation rate of the Pacific intermediate water during the last deglaciation. *Radiocarbon* **31**, 493–502 (1989).
91. K. Minoshima, H. Kawahata, T. Irino, K. Ikehara, K. Aoki, M. Uchida, M. Yoneda, Y. Shibata, Deep water ventilation in the northwestern North Pacific during the last deglaciation and the early Holocene (15-5 cal. kyr B.P.) based on AMS ^{14}C dating. *Nucl. Instrum. Methods Phys. Res. Sect. B* **259**, 448–452 (2007).
92. A. VanGeen, R. G. Fairbanks, P. Dartnell, M. McGann, J. V. Gardner, M. Kashgarian, Ventilation changes in the northeast Pacific during the Last Deglaciation. *Paleoceanography* **11**, 519–528 (1996).
93. K. Ikehara, T. Danhara, T. Yamashita, M. Tanahashi, S. Morita, K. Ohkushi, Paleoceanographic control on a large marine reservoir effect offshore of Tokai, south of Japan, NW Pacific, during the last glacial maximum-deglaciation. *Quat. Int.* **246**, 213–221 (2011).
94. P. A. Rafter, J.-C. Herguera, J. R. Southon, Extreme lowering of deglacial seawater radiocarbon recorded by both epifaunal and infaunal benthic foraminifera in a wood-dated sediment core. *Clim. Past* **14**, 1977–1989 (2018).
95. M. Sarnthein, P. M. Grootes, J. P. Kennett, M.-J. Nadeau, ^{14}C reservoir ages show deglacial changes in ocean currents and carbon cycle, in *Ocean Circulation: Mechanisms and Impacts—Past and Future Changes of Meridional Overturning* (Geophysical Monograph Series, American Geophysical Union, 2007), vol. 173, pp. 175–196.
96. S. Wan, Z. Jian, Deep water exchanges between the South China Sea and the Pacific since the last glacial period. *Paleoceanography* **29**, 1162–1178 (2014).
97. M. Sarnthein, S. Balmer, P. M. Grootes, M. Mudelsee, Planktic and benthic ^{14}C reservoir ages for three ocean basins, calibrated by a suite of ^{14}C Plateaus in the glacial-to-deglacial Suigetsu atmospheric ^{14}C record. *Radiocarbon* **57**, 129–151 (2016).
98. Y. Okazaki, K. Kimoto, H. Asahi, M. Sato, Y. Nakamura, N. Harada, Glacial to deglacial ventilation and productivity changes in the southern Okhotsk Sea. *Palaeogeogr. Palaeoclimatol. Palaeoecol.* **395**, 53–66 (2014).
99. S. C. Bova, T. D. Herbert, M. A. Altabet, Ventilation of northern and southern sources of aged carbon in the eastern equatorial Pacific during the younger dryas rise in atmospheric CO_2. *Paleoceanogr. Paleoclimatol.* **33**, 1151–1168 (2018).
100. C. M. Lindsay, S. J. Lehman, T. M. Marchitto, J. D. Carriquiry, J. D. Ortiz, New constraints on deglacial marine radiocarbon anomalies from a depth transect near Baja California. *Paleoceanography* **31**, 1103–1116 (2016).
101. A. Olsen, R. M. Key, S. Van Heuven, S. K. Lauvset, A. Velo, X. Lin, C. Schirnick, A. Kozyr, T. Tanhua, M. Hoppema, S. Jutterström, The Global Ocean Data Analysis Project version 2 (GLODAPv2)–an internally consistent data product for the world ocean. *Earth Syst. Sci. Data* **8**, (2016).
102. P. J. Reimer, E. Bard, A. Bayliss, J. W. Beck, P. G. Blackwell, C. B. Ramsey, C. E. Buck, H. Cheng, R. L. Edwards, M. Friedrich, P. M. Grootes, T. P. Guilderson, H. Haflidason, I. Hajdas, C. Hatté, T. J. Heaton, D. L. Hoffmann, A. G. Hogg, K. A. Hughen, K. F. Kaiser, B. Kromer, S. W. Manning, M. Niu, R. W. Reimer, D. A. Richards, E. M. Scott, J. R. Southon, R. A. Staff, C. S. M. Turney, J. van der Plicht, IntCal13 and Marine13 radiocarbon age calibration curves 0–50,000 years cal BP. *Radiocarbon* **55**, 1869–1887 (2013).
103. H. Kawahata, K.-i. Ohkushi, Y. Hatakeyama, Comparative Late Pleistocene paleoceanographic changes in the mid latitude boreal and austral western Pacific. *J. Oceanogr.* **55**, 747–761 (1999).
104. L. Maeda, H. Kawahata, M. Nohara, Fluctuation of biogenic and abiogenic sedimentation on the Shatsky Rise in the western North Pacific during the late Quaternary. *Mar. Geol.* **189**, 197–214 (2002).
105. I. L. Hendy, T. F. Pedersen, J. P. Kennett, R. Tada, Intermittent existence of a southern Californian upwelling cell during submillennial climate change of the last 60 kyr. *Paleoceanography* **19**, (2004).
106. H. Kawahata, A. Suzuki, H. Ohta, Export fluxes in the Western Pacific Warm Pool. *Deep Sea Res. I Oceanogr. Res. Pap.* **47**, 2061–2091 (2000).
107. R. S. Ganeshram, T. F. Pedersen, Glacial-interglacial variability in upwelling and bioproductivity off NW Mexico: Implications for Quaternary paleoclimate. *Paleoceanography* **13**, 634–645 (1998).
108. L. D. Keigwin, G. A. Jones, P. N. Froelich, A 15,000 year paleoenvironmental record from Meiji Seamount, far northwestern Pacific. *Earth Planet. Sci. Lett.* **111**, 425–440 (1992).
109. S. A. Gorbarenko, Stable isotope and lithologic evidence of late-glacial and Holocene oceanography of the Northwestern Pacific and its marginal seas. *Quatern. Res.* **46**, 230–250 (1996).
110. B. G. Brunelle, D. M. Sigman, S. L. Jaccard, L. D. Keigwin, B. Plessen, G. Schettler, M. S. Cook, G. H. Haug, Glacial/interglacial changes in nutrient supply and stratification in the western subarctic North Pacific since the penultimate glacial maximum. *Quat. Sci. Rev.* **29**, 2579–2590 (2010).
111. Y. Okazaki, K. Takahashi, K. Katsuki, A. Ono, J. Hori, T. Sakamoto, M. Uchida, Y. Shibata, M. Ikehara, K. Aoki, Late Quaternary paleoceanographic changes in the southwestern Okhotsk Sea: Evidence from geochemical, radiolarian, and diatom records. *Deep Sea Res. II Top. Stud. Oceanogr.* **52**, 2332–2350 (2005).
112. K. Minoshima, H. Kawahata, K. Ikehara, Changes in biological production in the mixed water region (MWR) of the northwestern North Pacific during the last 27 kyr. *Palaeogeogr. Palaeoclimatol. Palaeoecol.* **254**, 430–447 (2007).
113. O. Seki, M. Ikehara, K. Kawamura, T. Nakatsuka, K. Ohnishi, M. Wakatsuchi, H. Narita, T. Sakamoto, Reconstruction of paleoproductivity in the Sea of Okhotsk over the last 30 kyr. *Paleoceanography* **19**, PA1016 (2004).
114. H. Narita, M. Sato, S. Tsunogai, M. Murayama, M. Ikehara, T. Nakatsuka, M. Wakatsuchi, N. Harada, Y. Ujiié, Biogenic opal indicating less productive northwestern North Pacific during the glacial ages. *Geophys. Res. Lett.* **29**, 22–1–22–4 (2002).

115. S. A. Gorbarenko, E. L. Goldberg, M. Kashgarian, T. A. Velivetskaya, S. P. Zakharkov, V. S. Pechnikov, A. A. Bosin, O. Y. Psheneva, E. D. Ivanova, Millennium scale environment changes of the Okhotsk Sea during last 80 kyr and their phase relationship with global climate changes. *J. Oceanogr.* **63**, 609–623 (2007).
116. S. A. Gorbarenko, T. A. Khusid, I. A. Basov, T. Oba, J. R. Southon, I. Koizumi, Glacial Holocene environment of the southeastern Okhotsk Sea: Evidence from geochemical and palaeontological data. *Palaeogeogr. Palaeoclimatol. Palaeoecol.* **177**, 237–263 (2002).
117. D. Nürnberg, R. Tiedemann, Environmental change in the Sea of Okhotsk during the last 1.1 million years. *Paleoceanography* **19**, PA4011 (2004).
118. B. G. Brunelle, D. M. Sigman, M. S. Cook, L. D. Keigwin, G. H. Haug, B. Plessen, G. Schettler, S. L. Jaccard, Evidence from diatom-bound nitrogen isotopes for subarctic Pacific stratification during the last ice age and a link to North Pacific denitrification changes. *Paleoceanography* **22**, PA1215 (2007).
119. E. Maier, M. Méheust, A. Abelmann, R. Gersonde, B. Chapligin, J. Ren, R. Stein, H. Meyer, R. Tiedemann, Deglacial subarctic Pacific surface water hydrography and nutrient dynamics and links to North Atlantic climate variability and atmospheric CO_2. *Paleoceanography* **30**, 949–968 (2015).
120. P. J. Lam, L. F. Robinson, J. Blusztajn, C. Li, M. S. Cook, J. F. McManus, L. D. Keigwin, Transient stratification as the cause of the North Pacific productivity spike during deglaciation. *Nat. Geosci.* **6**, 622–626 (2013).
121. K. P. Knudson, A. C. Ravelo, Enhanced subarctic Pacific stratification and nutrient utilization during glacials over the last 1.2 Myr. *Geophys. Res. Lett.* **42**, 9870–9879 (2015).
122. S. Kim, K. Takahashi, B.-K. Khim, Y. Kanematsu, H. Asahi, A. C. Ravelo, Biogenic opal production changes during the Mid-Pleistocene Transition in the Bering Sea (IODP Expedition 323 Site U1343). *Quatern. Res.* **81**, 151–157 (2014).
123. L. Rodríguez Sanz, P. G. Mortyn, J. C. Herguera, R. Zahn, Hydrographic changes in the tropical and extratropical Pacific during the last deglaciation. *Paleoceanography* **28**, 529–538 (2013).
124. M. A. Taylor, I. L. Hendy, D. K. Pak, Deglacial ocean warming and marine margin retreat of the Cordilleran Ice Sheet in the North Pacific Ocean. *Earth Planet. Sci. Lett.* **403**, 89–98 (2014).
125. T. Sagawa, K. Toyoda, T. Oba, Sea surface temperature record off central Japan since the Last Glacial Maximum using planktonic foraminiferal Mg/Ca thermometry. *J. Quat. Sci.* **21**, 63–73 (2005).
126. D. K. Pak, D. W. Lea, J. P. Kennett, Millennial scale changes in sea surface temperature and ocean circulation in the northeast Pacific, 10–60 kyr BP. *Paleoceanography* **27**, PA1212 (2012).
127. Y. Kubota, K. Kimoto, R. Tada, H. Oda, Y. Yokoyama, H. Matsuzaki, Variations of East Asian summer monsoon since the last deglaciation based on Mg/Ca and oxygen isotope of planktic foraminifera in the northern East China Sea. *Paleoceanography* **25**, PA4205 (2010).
128. N. Harada, N. Ahagon, M. Uchida, M. Murayama, Northward and southward migrations of frontal zones during the past 40 kyr in the Kuroshio-Oyashio transition area. *Geochem. Geophys. Geosyst.* **5**, Q09004 (2004).
129. N. Harada, M. Sato, A. Shiraishi, M. C. Honda, Characteristics of alkenone distributions in suspended and sinking particles in the northwestern North Pacific. *Geochim. Cosmochim.* **70**, 2045–2062 (2006).
130. N. Harada, M. Sato, T. Sakamoto, Freshwater impacts recorded in tetraunsaturated alkenones and alkenone sea surface temperatures from the Okhotsk Sea across millennial-scale cycles. *Paleoceanography* **23**, PA3201 (2008).
131. M. Inagaki, M. Yamamoto, Y. Igarashi, K. Ikehara, Biomarker records from core GH02-1030 off Tokachi in the northwestern Pacific over the last 23,000 years: Environmental changes during the last deglaciation. *J. Oceanogr.* **65**, 847–858 (2009).
132. T. D. Herbert, J. D. Schuffert, D. Andreasen, L. Heusser, M. Lyle, A. Mix, A. C. Ravelo, L. D. Stott, J. C. Herguera, Collapse of the California current during Glacial Maxima linked to climate change on land. *Science* **293**, 71–76 (2001).
133. K. Sawada, N. Handa, Variability of the path of the Kuroshio ocean current over the past 25,000 years. *Nature* **392**, 592–595 (1998).
134. M. Yamamoto, T. Oba, J. Shimamune, T. Ueshima, Orbital-scale anti-phase variation of sea surface temperature in mid-latitude North Pacific margins during the last 145,000 years. *Geophys. Res. Lett.* **31**, L16311 (2004).
135. D. Isono, M. Yamamoto, T. Irino, T. Oba, M. Murayama, T. Nakamura, H. Kawahata, The 1500-year climate oscillation in the midlatitude North Pacific during the Holocene. *Geology* **37**, 591–594 (2009).
136. W. R. Gray, D. Evans, Nonthermal influences on Mg/Ca in planktonic foraminifera: A review of culture studies and application to the last glacial maximum. *Paleoceanogr. Paleoclimatol.* **34**, 306–315 (2019).
137. J. E. Tierney, S. B. Malevich, W. Gray, L. Vetter, K. Thirumalai, Bayesian calibration of the Mg/Ca paleothermometer in planktic foraminifera. *Paleoceanogr. Paleoclimatol.* **34**, 2005–2030 (2019).
138. W. R. Gray, S. Weldeab, D. W. Lea, Y. Rosenthal, N. Gruber, B. Donner, G. Fischer, The effects of temperature, salinity, and the carbonate system on Mg/Ca in *Globigerinoides ruber* (white): A global sediment trap calibration. *Earth Planet. Sci. Lett.* **482**, 607–620 (2018).
139. M. Regenberg, A. Regenberg, D. Garbe-Schönberg, D. W. Lea, Global dissolution effects on planktonic foraminiferal Mg/Ca ratios controlled by the calcite-saturation state of bottom waters. *Paleoceanography* **29**, 127–142 (2014).
140. J. Yu, R. F. Anderson, Z. Jin, J. W. B. Rae, B. N. Opdyke, S. M. Eggins, Responses of the deep ocean carbonate system to carbon reorganization during the Last Glacial–interglacial cycle. *Quat. Sci. Rev.* **76**, 39–52 (2013).
141. F. G. Prahl, L. A. Muehlhausen, D. L. Zahnle, Further evaluation of long-chain alkenones as indicators of paleoceanographic conditions. *Geochim. Cosmochim. Acta* **52**, 2303–2310 (1988).
142. M. H. Conte, M.-A. Sicre, C. Rühlemann, J. C. Weber, S. Schulte, D. Schulz-Bull, T. Blanz, Global temperature calibration of the alkenone unsaturation index ($U^{K'}_{37}$) in surface waters and comparison with surface sediments. *Geochem. Geophys. Geosyst.* **7**, Q02005 (2006).
143. J. E. Tierney, M. P. Tingley, BAYSPLINE: A new calibration for the alkenone paleothermometer. *Paleoceanogr. Paleoclimatol.* **33**, 281–301 (2018).
144. S.-T. Kim, J. R. O'Neil, Equilibrium and nonequilibrium oxygen isotope effects in synthetic carbonates. *Geochim. Cosmochim. Acta* **61**, 3461–3475 (1997).
145. J. F. Adkins, K. McIntyre, D. P. Schrag, The salinity, temperature, and $\delta^{18}O$ of the glacial deep ocean. *Science* **298**, 1769–1773 (2002).
146. K. Lambeck, H. Rouby, A. Purcell, Y. Sun, M. Sambridge, Sea level and global ice volumes from the Last Glacial Maximum to the Holocene. *Proc. Natl. Acad. Sci. U.S.A.* **111**, 15296–15303 (2014).
147. S. A. Marcott, J. D. Shakun, P. U. Clark, A. C. Mix, A reconstruction of regional and global temperature for the past 11,300 years. *Science* **339**, 1198–1201 (2013).
148. R. C. Wills, T. Schneider, Stationary eddies and the zonal asymmetry of net precipitation and ocean freshwater forcing. *J. Climate* **28**, 5115–5133 (2015).
149. R. Schlitzer, *Ocean Data View* (Alfred Wegener Institute for Polar and Marine Research, 2004).
150. L. Cao, M. Eby, A. Ridgwell, K. Caldeira, D. Archer, A. Ishida, F. Joos, K. Matsumoto, U. Mikolajewicz, A. Mouchet, J. C. Orr, G.-K. Plattner, R. Schlitzer, K. Tokos, I. Totterdell, T. Tschumi, Y. Yamanaka, A. Yool, The role of ocean transport in the uptake of anthropogenic CO_2. *Biogeosciences* **6**, 375–390 (2009).
151. A. Ridgwell, I. Zondervan, J. C. Hargreaves, J. Bijma, T. M. Lenton, Assessing the potential long-term increase of oceanic fossil fuel CO_2 uptake due to CO_2-calcification feedback. *Biogeosciences* **4**, 481–492 (2007).
152. A. Tagliabue, O. Aumont, R. DeAth, J. P. Dunne, S. Dutkiewicz, E. Galbraith, K. Misumi, J. K. Moore, A. Ridgwell, E. Sherman, C. Stock, M. Vichi, C. Völker, A. Yool, How well do global ocean biogeochemistry models simulate dissolved iron distributions? *GBC*, 10.1002/2015GB005289 (2016).
153. L. Loulergue, A. Schilt, R. Spahni, V. Masson-Delmotte, T. Blunier, B. Lemieux, J.-M. Barnola, D. Raynaud, T. F. Stocker, J. Chappellaz, Orbital and millennial-scale features of atmospheric CH4 over the past 800,000 years. *Nature* **453**, 383–386 (2008).
154. E. Monnin, A. Indermühle, A. Dällenbach, J. Flückiger, B. Stauffer, T. F. Stocker, D. Raynaud, J.-M. Barnola, Atmospheric CO2 concentrations over the last glacial termination. *Science* **291**, 112–114 (2001).
155. A. Schilt, M. Baumgartner, J. Schwander, D. Buiron, E. Capron, J. Chappellaz, L. Loulergue, S. Schüpbach, R. Spahni, H. Fischer, T. F. Stocker, Atmospheric nitrous oxide during the last 140,000 years. *Earth Planet. Sci. Lett.* **300**, 33–43 (2010).
156. R. Marsh, A. Yool, T. M. Lenton, M. Y. Gulamali, N. R. Edwards, J. G. Shepherd, M. Krznaric, S. Newhouse, S. J. Cox, Bistability of the thermohaline circulation identified through comprehensive 2-parameter sweeps of an efficient climate model. *Climate Dynamics* **23**, 761–777 (2004).
157. N. R. Edwards, R. Marsh, Uncertainties due to transport-parameter sensitivity in an efficient 3-D ocean-climate model. *Climate Dynamics* **24**, 415–433 (2005).
158. J. W. B. Rae, W. S. Broecker, What fraction of the Pacific and Indian oceans' deep water is formed in the Southern Ocean? *Biogeosciences* **15**, 3779–3794 (2018).
159. N. Ducet, P. Y. Le Traon, Global high-resolution mapping of ocean circulation from TOPEX/Poseidon and ERS-1 and -2. *J. Geophys. Res.* **105**, 19477–19498 (2000).
160. T. M. Marchitto, W. B. Curry, J. Lynch-Stieglitz, S. P. Bryan, K. M. Cobb, D. C. Lund, Improved oxygen isotope temperature calibrations for cosmopolitan benthic foraminifera. *Geochim. Cosmochim. Acta* **130**, 1–11 (2014).
161. S. N. Wood, Fast stable restricted maximum likelihood and marginal likelihood estimation of semiparametric generalized linear models. *J. R. Stat. Soc. Ser. B* **73**, 3–36 (2011).
162. A. Schmittner, N. Gruber, A. C. Mix, R. M. Key, A. Tagliabue, T. K. Westberry, Biology and air-sea gas exchange controls on the distribution of carbon isotope ratios ($\delta^{13}C$) in the ocean. *Biogeosciences* **10**, 5793–5816 (2013).
163. G. L. Simpson, Modelling palaeoecological time series using generalised additive models. *Front. Ecol. Evol.* **6**, 149 (2018).
164. B. L. Otto-Bliesner, E. C. Brady, G. Clauzet, R. Tomas, S. Levis, Z. Kothavala, Last Glacial Maximum and Holocene climate in CCSM3. *J. Climate* **19**, 2526–2544 (2006).
165. I. Eisenman, C. M. Bitz, E. Tziperman, Rain driven by receding ice sheets as a cause of past climate change. *Paleoceanography* **24**, PA4209 (2009).

166. W. R. Peltier, Global glacial isostasy and the surface of the ice-age Earth: The ICE-5G (VM2) model and Grace. *Annu. Rev. Earth Planet. Sci.* **32**, 111–149 (2004).
167. E. Galbraith, C. de Lavergne, Response of a comprehensive climate model to a broad range of external forcings: Relevance for deep ocean ventilation and the development of late Cenozoic ice ages. *Climate Dynam.* **52**, 653–679 (2019).
168. R. F. Ivanovic, L. J. Gregoire, M. Kageyama, D. M. Roche, P. J. Valdes, A. Burke, R. Drummond, W. R. Peltier, L. Tarasov, Transient climate simulations of the deglaciation 21–9 thousand years before present (version 1) – PMIP4 Core experiment design and boundary conditions. *Geosci. Model Dev.* **9**, 2563–2587 (2016).

Acknowledgments: The ideas in this manuscript benefited from spirited discussions on the role of the North Pacific in past climates, beginning with a Leopoldina Symposium organized by M. Sarnthein and G. Haug. We thank L. Menviel and E. Galbraith for sharing model output. This work was substantially improved by the comments of several anonymous reviewers. **Funding:** This work was funded by NERC grant NE/N011716/1 to J.W.B.R., a NERC studentship to B.T., and NSF grant OPP 1643445 to I.E. A.R. acknowledges support from NSF grant 1736771. **Author contributions:** B.T., W.R.G., P.A.R., E.F.M.L., and J.W.B.R. compiled and analyzed the proxy data. J.W.B.R. and R.C.J.W. carried out box model calculations. R.C.J.W. and I.E. processed GCM model results. A.B., R.R.-O., M.F., and J.W.B.R. carried out cGENIE simulations, with assistance from A.R. J.W.B.R. and B.F. developed the ideas relating to Beringian habitability. All authors discussed the results and commented on the manuscript. **Competing interests:** The authors declare that they have no competing interests. **Data and materials availability:** Data presented in this paper are available as a supplementary data file accompanying this paper online, and on Pangaea, NCDC, and the NERC National Geoscience Data Centre. The cGENIE.muffin model code is hosted on GitHub and can be obtained by cloning: https://github.com/derpycode/cgenie.muffin. Configuration files for the specific experiments focused on in the paper can be found in the subdirectory: genie-userconfigs\MS\raetal.2020. Details of these experiments, plus the command line needed to run each one, are given in the readme.txt file in that directory. All other configuration files and boundary conditions are provided as part of the release. The complete ensemble of model experiments can be obtained by contacting the first author. Note that the specific version of the cGENIE.muffin code used to produce the model results in this paper is git revision: 8e340e5b171b7d86d3e47b0c163200fab623aa67.

Submitted 4 June 2020
Accepted 21 October 2020
Published 9 December 2020
10.1126/sciadv.abd1654

Citation: J. W. B. Rae, W. R. Gray, R. C. J. Wills, I. Eisenman, B. Fitzhugh, M. Fotheringham, E. F. M. Littley, P. A. Rafter, R. Rees-Owen, A. Ridgwell, B. Taylor, A. Burke, Overturning circulation, nutrient limitation, and warming in the Glacial North Pacific. *Sci. Adv.* **6**, eabd1654 (2020).